BAG6 supports stress fiber formation by preventing the ubiquitin-mediated degradation of RhoA

Maho Miyauchi, Reina Matsumura, and Hiroyuki Kawahara*
Laboratory of Cell Biology and Biochemistry, Department of Biological Sciences, Tokyo Metropolitan University, Tokyo 192-0397, Japan

ABSTRACT **The Rho family of small GTPases is a key regulator of cytoskeletal actin polymerization. Although the ubiquitination of Rho proteins is reported to control their activity, the mechanisms by which the ubiquitination of Rho family proteins is controlled by ubiquitin ligases have yet to be elucidated. In this study, we identified BAG6 as the first factor needed to prevent the ubiquitination of RhoA, a critical Rho family protein in F-actin polymerization. We found that BAG6 is necessary for stress fiber formation by stabilizing endogenous RhoA. BAG6 deficiency enhanced the association between RhoA and Cullin-3-based ubiquitin ligases, thus promoting its polyubiquitination and subsequent degradation, leading to the abrogation of actin polymerization. In contrast, the restoration of RhoA expression through transient overexpression rescued the stress fiber formation defects induced by BAG6 depletion. BAG6 was also necessary for the appropriate assembly of focal adhesions as well as cell migration events. These findings reveal a novel role for BAG6 in maintaining the integrity of actin fiber polymerization and establish BAG6 as a RhoA-stabilizing holdase, which binds to and supports the function of RhoA.**

Monitoring Editor
Stephanie Gupton
University of North Carolina, Chapel Hill

Received: Aug 22, 2022
Revised: Feb 17, 2023
Accepted: Feb 27, 2023

INTRODUCTION

The dynamics of the actin cytoskeletal architecture are regulated at the level of actin polymerization. The Rho family of small GTPases (e.g., RhoA, Rac1, and CDC42) is a key regulator of distinct steps of cytoskeletal actin polymerization as well as the interaction of actin fibers with cell adhesion molecules (Ridley *et al.*, 1992; Nobes and Hall, 1995; Hall, 1998; Etienne-Manneville and Hall, 2002; Jaffe and Hall, 2005; Heasman and Ridley, 2008). For example, Rac1 or CDC42 activation induces the actin-mediated formation of membrane protrusions (Ridley *et al.*, 1992; Nobes and Hall, 1995; Hall, 1998; Heasman and Ridley, 2008), whereas the activation of RhoA in the cell body induces the assembly of contractile F-actin and myosin filament structures called stress fibers and the assembly of focal adhesions (FAs) (Ridley and Hall, 1992; Hall 1998; Wang *et al.*, 2003). RhoA activity must be controlled strictly because it may also influence cell migration, adhesion, polarization, invasion, and tumor metastasis by increasing the number of stress fiber-dependent adhesions to the substrate (Sahai and Marshall, 2002; Vial *et al.*, 2003; Wang *et al.*, 2003; Sahai *et al.*, 2007; Vega and Ridley, 2008; Fonseca *et al.*, 2010; Maeda *et al.*, 2011; Anne, 2015). Therefore it is critical to identify the regulatory network of Rho family small GTPases.

Rho family proteins control actin polymerization by cycling between their active GTP-bound and inactive GDP-bound forms (Bishop and Hall, 2000). GTP hydrolysis induces conformational changes of the GTPase domain, especially within short specific regions called Switch I and Switch II (Wei *et al.*, 1997; Hall, 1998; Vetter and Wittinghofer, 2001; Jaffe and Hall, 2005; Schaefer *et al.*, 2014); thus GTP hydrolysis induces the subsequent inactivation of Rho proteins (Ridley and Hall, 1992). Posttranslational modifications such as ubiquitination and phosphorylation are also reported to regulate the activity and stability of Rho GTPases (Bryan *et al.*, 2005; Boyer *et al.*, 2006; Chen *et al.*, 2009; Nethe and Hordijk, 2010;

This article was published online ahead of print in MBoC in Press (http://www.molbiolcell.org/cgi/doi/10.1091/mbc.E22-08-0355) on March 8, 2023.

Author contributions: M.M. and H.K. conceived and designed the experiments, M.M. and R.M. performed the experiments, and M.M. and H.K. wrote the paper.

Conflict of interest: The authors declare that there are no competing commercial interests in relation to this work.

*Address correspondence to. Hiroyuki Kawahara (hkawa@tmu.ac.jp).

Abbreviations used: CHX, cycloheximide; FA, focal adhesion; GDP, guanosine diphosphate; GTP, guanosine triphosphate; IP, immunoprecipitation; siRNAs, small interfering RNAs; WT, wild-type.

Torrino *et al.*, 2011; Ding *et al.*, 2011; Schaefer *et al.*, 2014; Kovacevic *et al.*, 2018; Lin *et al.*, 2022). Although RhoB is a short-lived protein with a half-life of 1–2 h (Lebowitz *et al.*, 1995), the half-life of RhoA is relatively long. The elimination of RhoA in HeLa cells is controlled mainly by Cullin-3 (CUL3)-based E3 ubiquitin ligases for proteasomal degradation, and the depletion of CUL3 results in the stabilization and massive accumulation of RhoA (Chen *et al.*, 2009; Kovacevic *et al.*, 2018). However, the regulatory mechanisms by which the ubiquitination of Rho family proteins is controlled by CUL3-based ubiquitin ligases remain to be elucidated.

In this study, we identified BAG6 as the first factor needed to stabilize endogenous RhoA. BAG6 (also called BAT3 or Scythe) is a chaperonelike protein that possesses an intrinsic affinity for the hydrophobic residues of client proteins (Kikukawa *et al.*, 2005; Mariappan *et al.*, 2010; Minami *et al.*, 2010; Wang *et al.*, 2011; Tanaka *et al.*, 2016). BAG6 recognizes newly synthesized transmembrane domain proteins in the cytosol for subsequent degradation when their proper biogenesis has failed, thus participating in protein quality control (Minami *et al.*, 2010; Hessa *et al.*, 2011; Kawahara *et al.*, 2013; Lee and Ye, 2013; Payapilly and High, 2014; Kaudeer and Koch, 2014; Suzuki and Kawahara, 2016; Guna and Hegde, 2018). In contrast with these previously reported functions of BAG6, the findings of the present study suggest that a deficiency in BAG6 results in the destabilization of endogenous RhoA protein, leading to the abrogation of stress fiber formation. We found that BAG6 depletion enhanced the association between RhoA and CUL3-based ubiquitin ligases, thereby promoting its polyubiquitination and subsequent degradation. In contrast, the restoration of RhoA expression via its transient overexpression rescued the defects in stress fiber formation induced by BAG6 depletion, bypassing the requirement for BAG6. BAG6 was also necessary for the appropriate assembly of FAs as well as cell migration events. These findings reveal a novel role for BAG6 in maintaining the integrity of actin fiber polymerization by preventing the excess ubiquitination of RhoA.

RESULTS

BAG6 physically interacts with RhoA

The small GTPase Rab8a in its GDP-bound form has been found to associate with BAG6, and BAG6 targets Rab8a for ubiquitin-dependent degradation (Takahashi *et al.*, 2019). Because Rho family small GTPases are reported to be degraded by the ubiquitin-dependent pathway (Doye *et al.*, 2002; Wang *et al.*, 2003; Boyer *et al.*, 2006; Chen *et al.*, 2009; Nethe and Hordijk, 2010; Ding *et al.*, 2011), we examined whether BAG6 physically associates with Rho family GTPases. As shown in Figure 1A, Flag-tagged RhoA was coimmunoprecipitated with BAG6 from HeLa cell extracts. In contrast, the closely related Rho family small GTPase Rac1 did not coprecipitate with BAG6, and CDC42 showed marginal affinity with BAG6 under identical conditions (Figure 1, A and B). Deletion of the N-terminal 465 residues of BAG6, a hydrophobicity recognition region of this chaperonelike protein (Tanaka *et al.*, 2016), abolished its interaction with RhoA (ΔN465, Supplemental Figure S1A). These results suggest that the N-terminus of BAG6 possesses a higher binding affinity for RhoA than for other Rho family small GTPases.

BAG6 has been shown to recognize the Rab family of small GTPases in a nucleotide-specific manner, and the GDP-bound inactive form of Rab8a coimmunoprecipitates with BAG6, whereas its GTP-bound form is scarcely recognized (Takahashi *et al.*, 2019). To examine the nucleotide dependency of Rho GTPases for their interaction with BAG6, we prepared constitutively active GTP-bound mutants (Q63L for RhoA, Q61L for Rac1) and inactive GDP-bound mutants (T19N for RhoA, T17N for Rac1).

Similar to the case for Rab8a (Takahashi *et al.*, 2019), we found that BAG6 predominantly interacted with the GDP-bound form of RhoA-T19N, whereas BAG6 showed reduced affinity for constitutively active GTP-bound RhoA-Q63L as well as its wild-type (WT) form (Figure 1, C and D). BAG6 did not show any detectable affinity for Rac1 irrespective of its nucleotide-bound status (Figure 1C). These observations suggest that BAG6 possesses a higher affinity for RhoA, especially in its GDP-bound form, than for other Rho family members. Therefore we focused on the roles of BAG6 in the cellular function of RhoA.

BAG6 depletion induces defects in stress fiber formation

RhoA is known to promote the assembly of contractile F-actin stress fibers (Ridley and Hall, 1992). Because we found that BAG6 interacted with RhoA, we examined the possible participation of BAG6 in actin fiber polymerization. Staining of HeLa cells with Texas Red-labeled phalloidin, a specific marker for polymerized actin (F-actin), detected fiberlike structures (stress fibers) in the cytoplasm (Figure 2Aa, see also Supplemental Figure S1Ba). Treatment with cytochalasin D, an inhibitor of actin polymerization, abolished the fiberlike phalloidin signals (Supplemental Figure S1Bc). In contrast, depletion of CUL3, a ubiquitin ligase component responsible for RhoA degradation, stimulated excess stress fiber formation, as previously reported (Figure 2Ab) (Chen *et al.*, 2009). Importantly, BAG6 knockdown with two independent double-stranded small interfering RNAs (siRNAs #1 and #8) also inhibited F-actin stress fiber formation (Figure 2A,c and d) to a similar level as observed for cytochalasin D treatment (Supplemental Figure S1B, b and c). We verified the knockdown efficacies of the respective siRNAs by Western blot analysis (Figure 2B). To quantify the population of cells with defective actin fiber polymerization, we measured the fluorescence intensity of phalloidin-iFluor 488 signals by flow cytometry (Kopitar *et al.*, 2019). This analysis supported the significant reduction of F-actin polymerization signals in BAG6-depleted cells (Figure 2, C and D).

BAG6 is reported to be a component of the protein ubiquitination machinery responsible for pre-emptive protein quality control (Hessa *et al.*, 2011; Rodrigo-Brenni *et al.*, 2014; Suzuki and Kawahara, 2016; Guna and Hegde, 2018). Since Rab8a degradation is enhanced by the components of the pre-emptive protein quality control system, we examined whether these BAG6-associated proteins also modulated F-actin stress fiber formation. Depletion of components of the pre-emptive protein quality control system (Supplemental Figure S2, A and B), including UBQLN4, RNF126, and RNF115, did not decrease stress fiber formation compared with control depleted cells (Figure 3, A–D). In contrast, BAG6 depletion reproducibly abolished stress fiber formation (Figure 3E). Because BAG6 is also a component of the tail-anchored protein biogenesis machinery (Leznicki *et al.*, 2010; Mariappan *et al.*, 2010), we depleted the BAG6-associated TRC complex protein UBL4A, a homolog of yeast GET5 (Supplemental Figure S2, A and B)(Mariappan *et al.*, 2010; Kuwabara *et al.*, 2015). We found that UBL4A knockdown did not reduce cytoplasmic stress fiber formation in HeLa cells (Figure 3F). These observations suggest that BAG6 possesses a unique role in the formation of stress fibers independent of its known functions in pre-emptive protein quality control and tail-anchored protein biogenesis.

RhoA-mediated stress fiber formation is critical for neural cell morphology (Dupraz *et al.*, 2019). Therefore we examined the effect of BAG6 depletion on F-actin oligomerization in SH-SY5Y cells, a human neuroblastoma cell line. We found that BAG6 knockdown with two independent siRNA duplexes (#1 and #6) resulted in defective actin polymerization (Supplemental Figure S3A) and reduced

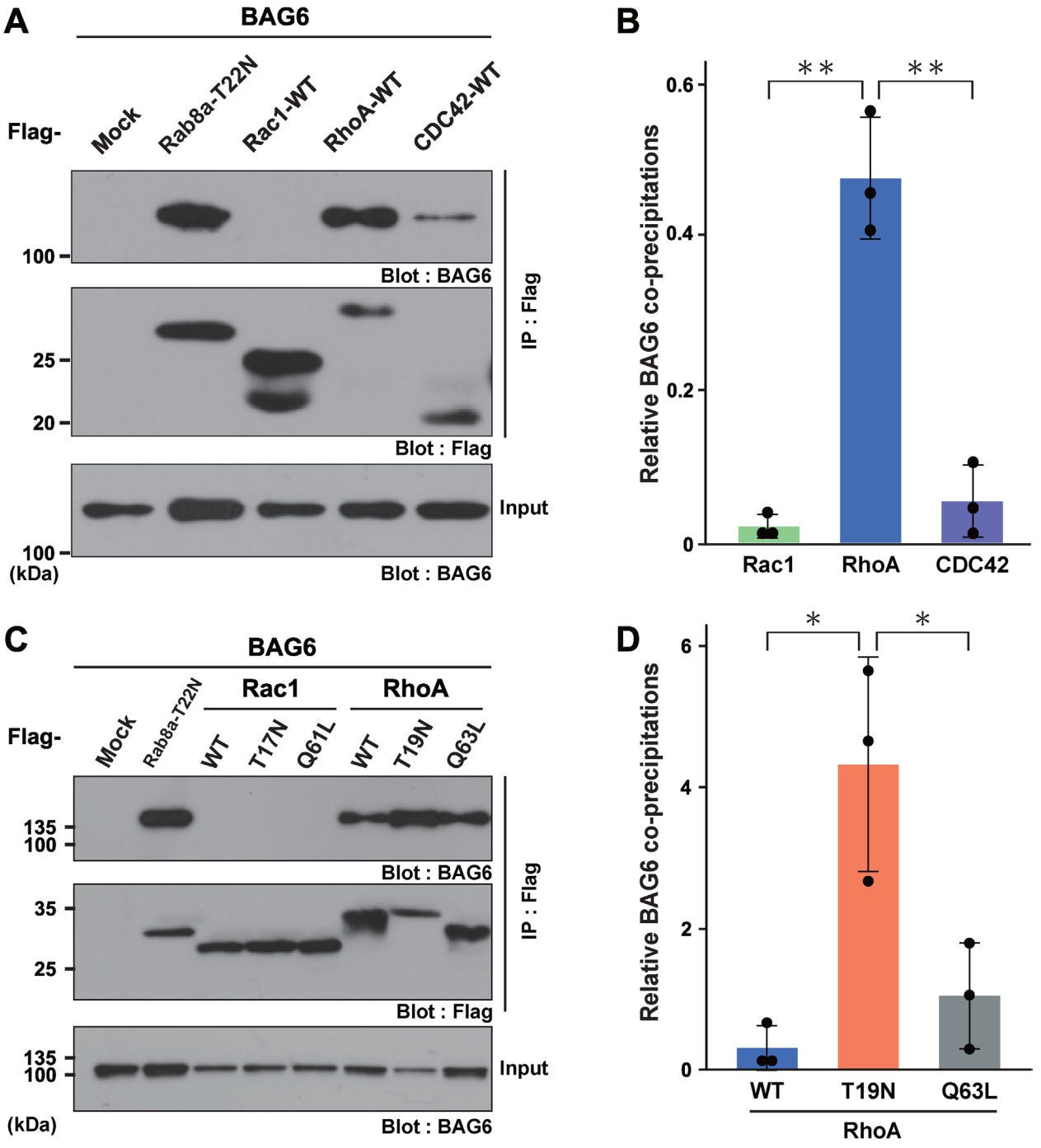

FIGURE 1: BAG6 physically interacts with RhoA. (A, B) WT Rac1, RhoA, and CDC42 proteins with N-terminal Flag-tags were coexpressed with BAG6 in HeLa cells. Flag-tagged immunoprecipitates (IP) were blotted with anti-BAG6 and anti-Flag antibodies as indicated. The GDP-bound Rab8a-T22N mutant was used as a positive control for BAG6 interactions. Mock indicates cells with empty vector transfection as a negative control. All cells were treated with 10 μM MG-132 for 4 h before harvest. The graph in B shows the relative signal intensities of coprecipitated Rho family small GTPases with BAG6 (signal intensities of the BAG6 blot were divided by those of the Flag blot). $^{**}p < 0.01$ (Student's *t* test). (C, D) Flag-tagged RhoA and Rac1 were expressed with BAG6 in HeLa cells, and their Flag-precipitates were probed with an anti-BAG6 antibody. Constitutively active GTP-bound mutants (Rac1-Q61L and RhoA-Q63L) and inactive GDP-bound mutants (Rac1-T17N and RhoA-T19N) were used to examine the nucleotide dependency of these small GTPases to bind with BAG6. All cells were treated with 10 μM MG-132 for 4 h before harvest. The graph in D shows the relative signal intensities of coprecipitated RhoA with BAG6. $^{*}p < 0.05$ (Student's *t* test).

the formation of membrane protrusions (Supplemental Figure S3B), suggesting that BAG6 might be crucial for maintaining neural cell morphology.

BAG6 deficiency impairs the formation of FAs

Cells lacking CUL3 are reported to show the increased formation of FAs on which stress fibers are anchored (Genau *et al.*, 2015). Since

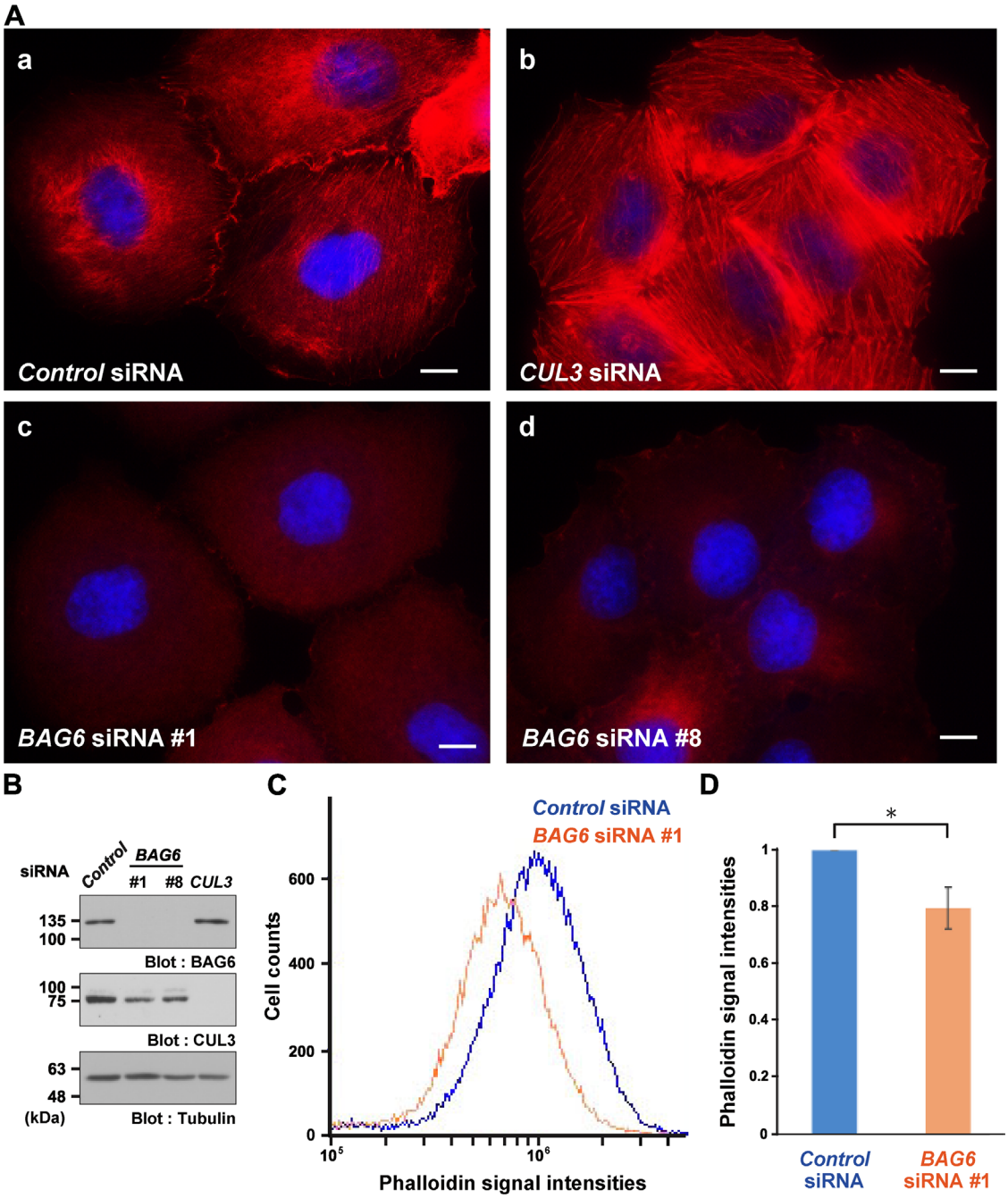

FIGURE 2: BAG6 depletion induces defects in stress fiber formation. (A) At 48 h after transfection with 10 nM siRNA duplexes for control (a), *CUL3* (b), or *BAG6* (siRNA target sequences #1 [c] and #8 [d]), HeLa cells were stained with Texas Red-labeled phalloidin (shown as red signals). Note that the exposure times of all photographs in this figure were identical, indicating that the signal intensities correspond to the degree of cytoplasmic actin polymerization. Scale bar: 10 µm. See also Supplemental Figure S1B. (B) Knockdown efficacies of endogenous BAG6 and CUL3 in this experiment were verified by Western blot analysis with specific antibodies. (C, D) Flow cytometric analysis of actin fiber polymerization. Fluorescent signals derived from phalloidin-iFluor 488 staining in the control or BAG6 siRNA#1 duplex-treated HeLa cells were quantified. The data were obtained by log scale analysis. The flow cytometry pattern of negative control siRNA is indicated as a blue line, and after treatment with *BAG6* siRNA is indicated with an orange line (C). Quantitative evaluation of the mean fluorescence intensity of phalloidin-iFluor 488-stained cells (D). The value of the control siRNA was defined as 1.0. The graph represents the mean ± SD calculated from three independent biological replicates. *$p < 0.05$ (Student's *t* test).

BAG6 knockdown induced defects in stress fiber formation (Figure 2), we examined whether the formation of FAs was affected in BAG6-depleted cells. The number and size of FAs can be monitored by staining with paxillin, which is a well-established marker of FAs (Kovacevic *et al.*, 2018). We found that BAG6 depletion reduced the formation of paxillin foci (Figure 4A, a and b, see also Supplemental Figure S4), concomitant with the defective formation of stress fibers (Figure 4A, c and d). Merged images of paxillin/phalloidin

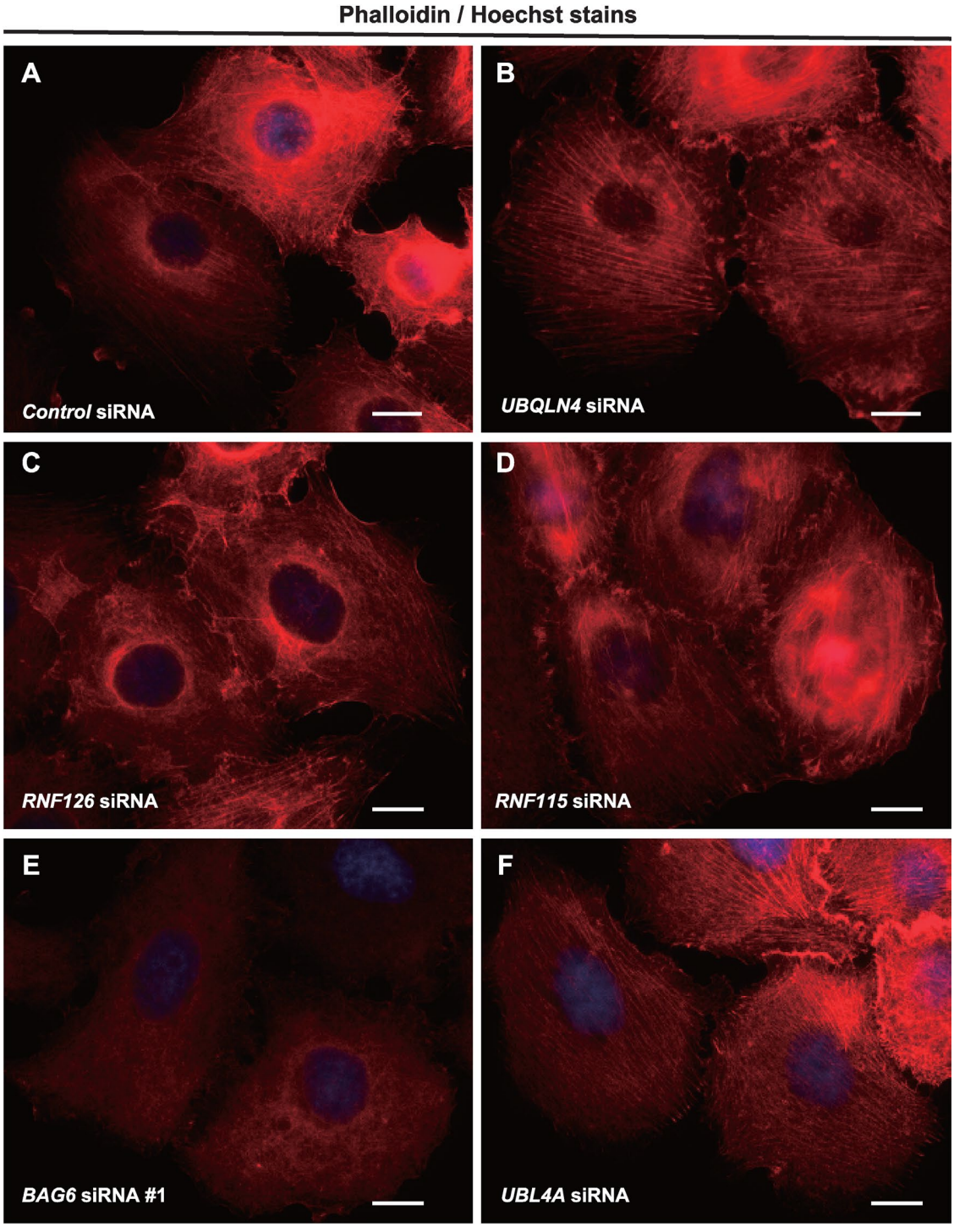

FIGURE 3: Depletion of BAG6-associated proteins does not down-regulate stress fiber formation. At 48 h after transfection with siRNA duplexes for control (A), *UBQLN4* (B), *RNF126* (C), *RNF115* (D), *BAG6* #1 (E), and *UBL4A* (F) (10 nM each), HeLa cells were stained for F-actin (shown as red) with Texas Red-labeled phalloidin. Nuclei were stained with Hoechst 33342 (shown as blue). Scale bar: 10 µm. Note that all images presented in this figure were acquired in an identical set of experiments, and the exposure times of all photographs in this figure were the same. Independent experiments were repeated twice to ensure the reproducibility of the data. See also Supplemental Figure S2.

double-stained cells showed that actin fiber-linked FAs were reduced in BAG6-depleted cells (Figure 4B). There was a shift in the distribution of paxillin foci from a centralized pattern in control cells to a more peripheral distribution in BAG6 knockdown cells. Quantitative analyses of FAs also supported the significant decrease in the number (paxillin-positive foci per cell) and size (paxillin-positive area per FA) of FAs in BAG6-depleted cells (Figure 4, C–E). These observations suggest that BAG6 depletion compromises not only the formation of stress fibers but also the number and size of FAs in HeLa cells.

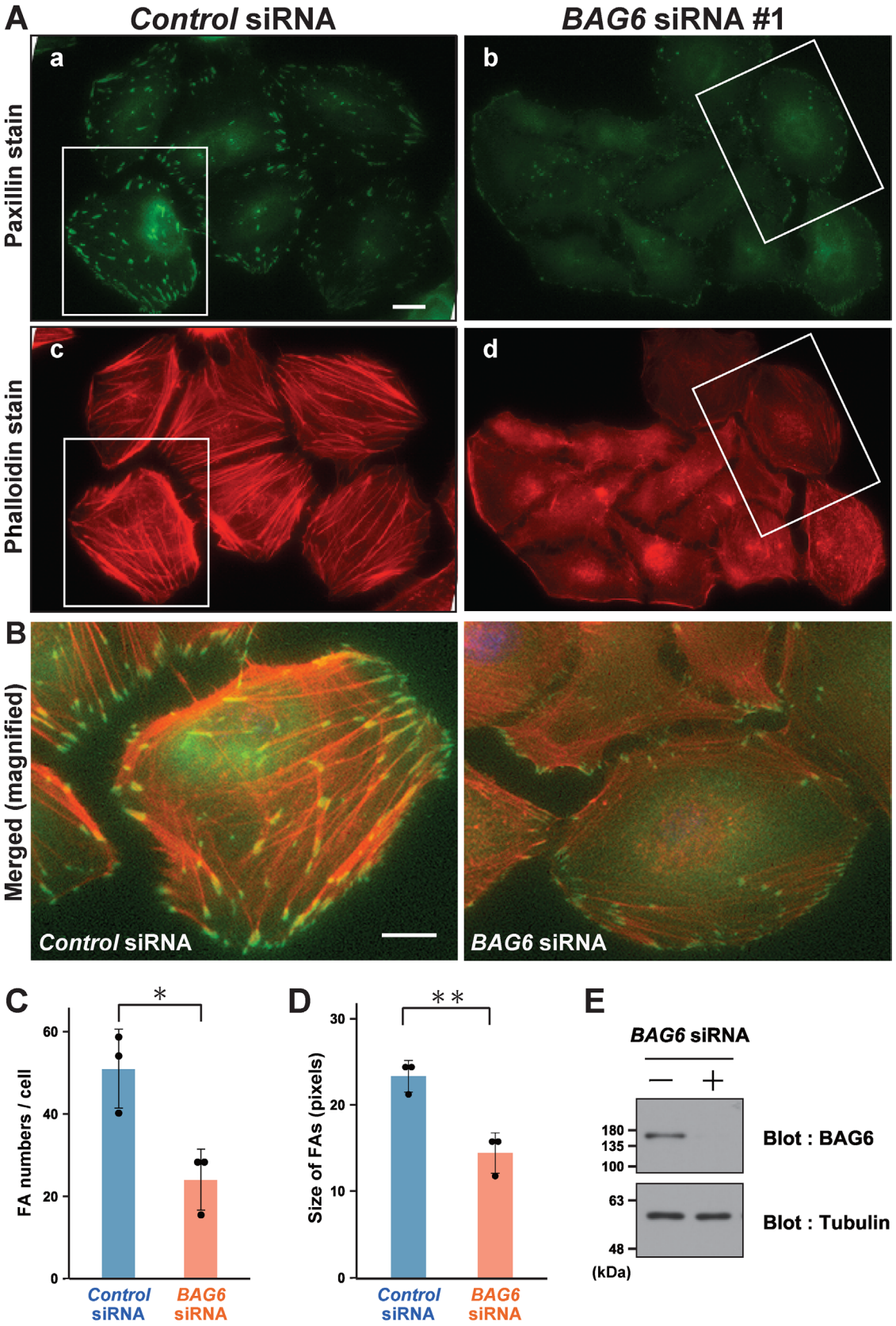

FIGURE 4: BAG6 deficiency impairs FA formation. (A) BAG6 depletion impairs FA in HeLa cells. Representative images of anti-paxillin immunofluorescence staining for FAs (a, b, shown as green) and Texas Red-labeled phalloidin staining for F-actin filaments (c, d, shown as red). Note that all images presented in this figure were acquired in an identical set of experiments. Magnified areas in B are indicated by white lines. Scale bar: 20 μm. (B) Merged and magnified images of paxillin (shown as green) and stress fiber (shown as red) staining. Scale bar: 10 μm. (C, D) The number of FAs

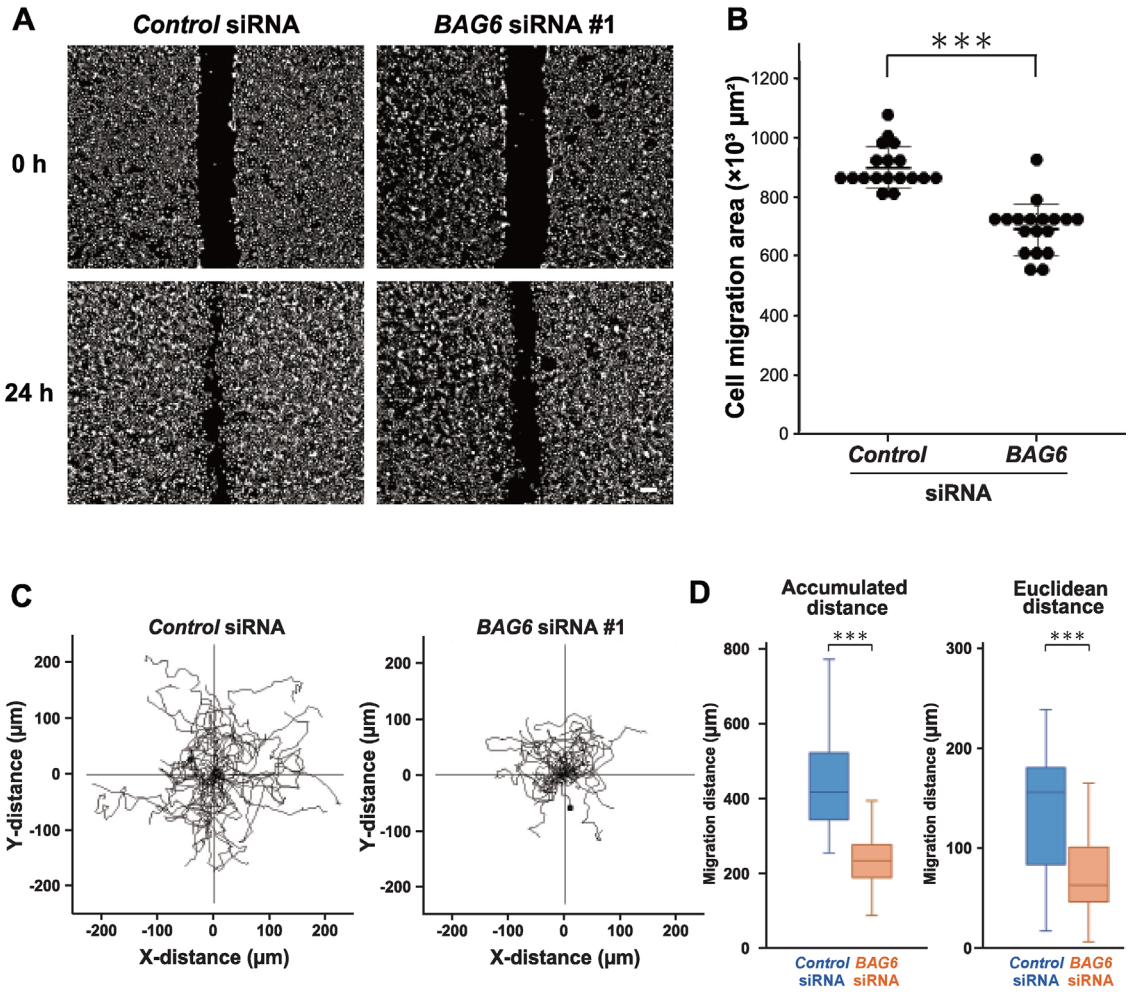

FIGURE 5: BAG6 knockdown attenuates cell migration. (A) Wound-healing assay evaluating the cell migration defects induced by BAG6 depletion with *BAG6* siRNA duplex #1. Photographs were taken at 0 and 24 h after wounding to observe and measure cell migration quantitatively. HeLa cells were treated with 3 µg/ml mitomycin C for 1 h before scratching to block further cell proliferation. Scale bar: 200 µm. (B) The extent of cell migration was determined by ImageJ software. The graph represents mean values ± SD (thick horizontal lines), confidence limits (thin horizontal lines), and coefficients of variation (label) calculated from biologically independent replicates (control cells, $n = 18$; *BAG6* knockdown cells, $n = 18$). ***$p < 0.001$ (Student's *t* test). (C) Cell migration evaluation by two-dimensional phase contrast video microscopy and single-cell tracking analysis (8-h video recorded between 48 and 56 h post-siRNA duplex transfection, 10-min intervals) of MDA-231 cells with control or BAG6 depletion. Wind-rose plots with cell tracks for control and BAG6-depleted cells. Migration distances were measured from each of 10 cells in three independent experiments. See also Supplemental Movies S1–S4. (D) Box-whisker plots present accumulated distance and Euclidean distance of the tracked cells. The error bars indicate the minimum and maximum values for the data sets. ***$p < 0.001$ (Student's *t* test).

BAG6 knockdown attenuates cell migration

Cell migration is a key process in many physiological and pathological processes, including wound healing, morphogenesis, and cancer metastasis (Sahai and Marshall, 2002; Vega and Ridley, 2008; Chen *et al.*, 2009; Anne, 2015; Ridley, 2015; Haga and Ridley, 2016). The excess or deficient formation of stress fibers and FAs is associated with a reduction of cell migration (Fonseca *et al.*, 2010; Ridley, 2015). Since BAG6 was found to be necessary for stress fiber formation (Figure 2) and FA assembly in HeLa cells (Figure 4), we examined whether the ability of cells to migrate was attenuated in the absence of BAG6. Two separated layers of cells, which were pretreated with mitomycin C to block further cell proliferation, were monitored to examine cell movement within 24 h after wound formation. This wound-healing assay showed that siRNA knockdown of

(paxillin-positive foci) per cell (C) and the paxillin-positive area (counted as the number of green pixels) per FA (D) were analyzed using the particle analysis function of ImageJ software. The dots in the graphs represent the averages of three independent biological replicates (number of counted cells: control = 59, 113, and 88; *BAG6* knockdown = 60, 71, and 104). *$p < 0.05$, **$p < 0.01$ (Student's *t* test). (E) Knockdown efficacy of endogenous BAG6 in this experiment was verified by Western blot analysis with an anti-BAG6 antibody.

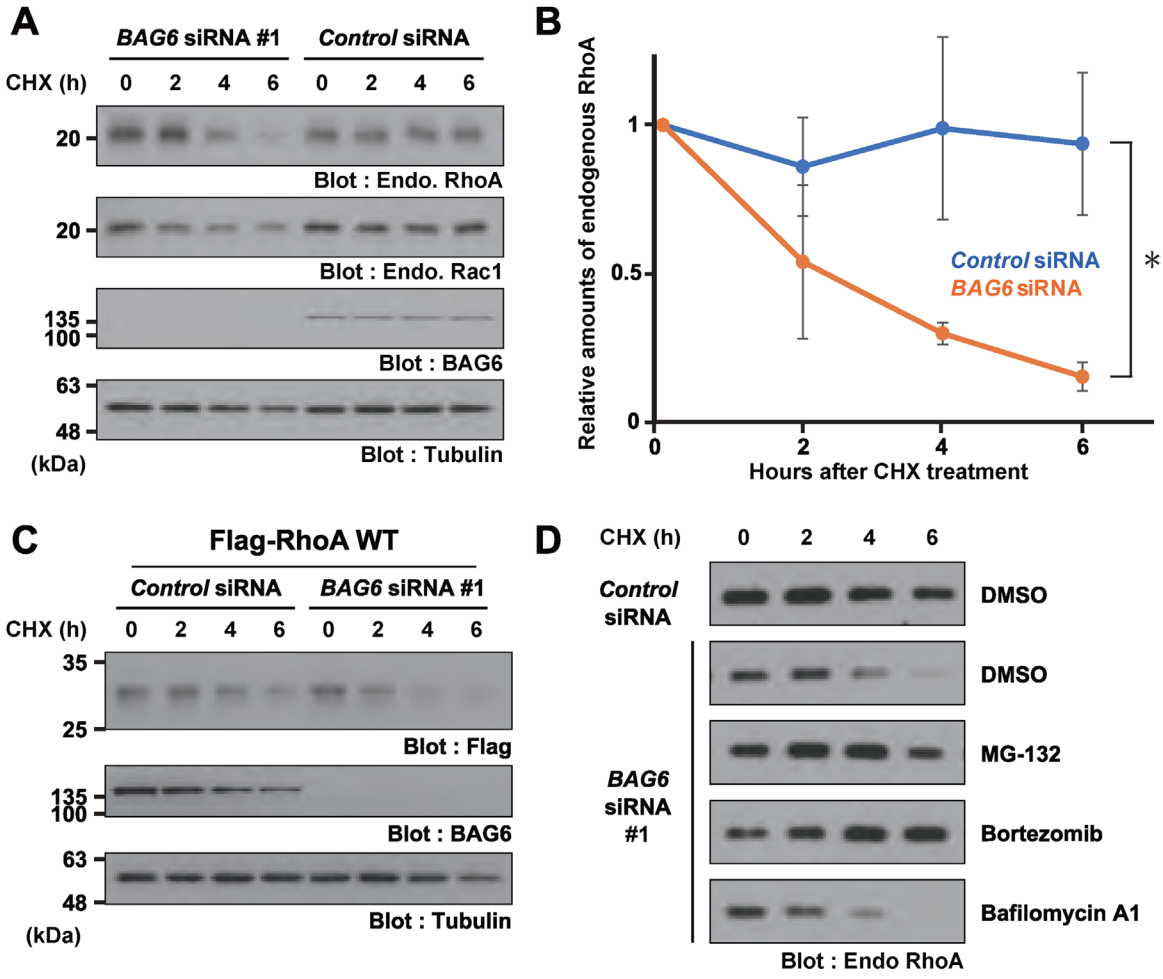
A
BAG6 siRNA #1
Control siRNA
CHX (h)
0 2 4 6 0 2 4 6
20
Blot : Endo. RhoA
20
Blot : Endo. Rac1
135
100
Blot : BAG6
63
48
(kDa)
Blot : Tubulin
B
Relative amounts of endogenous RhoA
1
0.5
0
Control siRNA
BAG6 siRNA
*
0 2 4 6
Hours after CHX treatment
C
Flag-RhoA WT
Control siRNA
BAG6 siRNA #1
CHX (h)
0 2 4 6 0 2 4 6
35
25
Blot : Flag
135
100
Blot : BAG6
63
48
(kDa)
Blot : Tubulin
D
CHX (h)
0 2 4 6
Control siRNA
DMSO
BAG6 siRNA #1
DMSO
MG-132
Bortezomib
Bafilomycin A1
Blot : Endo RhoA
E
BAG6 depleted HeLa cells
Phalloidin stain
Merged with Flag stain (green)

BAG6 led to significantly reduced cell migration (Figure 5, A and B). This observation implies that BAG6 might play a role in cell migration.

BAG6 silencing reduces single-cell migration of breast cancer cells

To investigate cell migration more quantitatively, we turned to two-dimensional video microscopy of low-density cell cultures followed by single-cell tracking (Blockhuys *et al.*, 2020). In this experiment, we analyzed the highly invasive human breast cancer cell line MDA-MB-231 (i.e., MDA-231 cells). Tracking of MDA-231 cells for 8 h (Figure 5C, examples of tracking data are given in Supplemental Movies S1–S4) revealed that BAG6-depleted cells had less distributed tracks compared with control cells. Specifically, quantitative analysis showed that BAG6-depleted cells migrated with a shorter accumulated distance (median accumulated distance: control siRNA, 418.5 μm vs. BAG6 siRNA, 235.2 μm, Figure 5D, left panel, and median Euclidean distance: control siRNA, 156.1 μm vs. BAG6 siRNA, 62.8 μm, Figure 5D, right panel). These results suggest that MDA-231 cell migration is suppressed upon BAG6 silencing.

Stability of endogenous RhoA is dependent on BAG6

To gain insight into the mechanism by which BAG6 regulates stress fiber formation and cell migration, we focused on the stability of RhoA because BAG6 is reported to regulate the degradation of the Rab-family small GTPases (Takahashi *et al.*, 2019). To investigate the contribution of BAG6 to RhoA degradation, we compared the stability of endogenous RhoA in the presence or absence of *BAG6* siRNA. Although cycloheximide (CHX) chase experiments confirmed that the majority of endogenous RhoA was highly stable in HeLa cells (Figure 6A, *control* siRNA, see also Supplemental Figure S5A), the stability of endogenous RhoA was markedly reduced in BAG6-depleted cells (Figures 6A, *BAG6* siRNA, see also Supplemental Figure S5A) with a half-life of less than 3 h (Figure 6B). Similarly, BAG6 depletion made exogenously expressed WT Flag-tagged RhoA, also known as a stable protein, unstable (Figure 6C). RhoC, a close paralog of human RhoA, was also destabilized by BAG6 depletion (Supplemental Figure S5B). Because the exogenous expression system used was driven by a constitutive promoter, the instability of Flag-tagged RhoA and RhoC in BAG6-depleted cells was not due to transcriptional or epigenetic silencing. Thus BAG6 is required for the stable expression of RhoA family proteins, contrary to the previously reported pro-degradation functions of BAG6 for Rab family small GTPases (Takahashi *et al.*, 2019) and mislocalized transmembrane proteins (Minami *et al.*, 2010; Hessa *et al.*, 2011; Wang *et al.*, 2011, Kamikubo *et al.*, 2019).

The degradation of endogenous RhoA induced by BAG6 depletion was blocked by MG-132, a broad specificity inhibitor of intracellular proteinases (Figure 6D). The proteasome-specific inhibitor bortezomib also inhibited the BAG6 depletion-mediated destabilization of RhoA, while the lysosome inhibitor bafilomycin A1 did not (Figure 6D). Collectively, these results suggest that the proteasome is responsible for BAG6 depletion-induced RhoA degradation, and BAG6 is necessary for the stabilization of endogenous RhoA protein to support actin polymerization.

Expression of exogeneous RhoA rescues defects in stress fiber formation in BAG6-depleted cells

Because BAG6 depletion induced the degradation of the endogenous pool of RhoA (Figure 6, A–D), we next examined whether the forced expression of RhoA could rescue stress fiber formation in BAG6-depleted cells. The forced expression of Flag-tagged RhoA (shown as green signals) rescued the defects in stress fiber formation in BAG6 knockdown cells (Figure 6E, indicated by white arrowheads), whereas cells lacking exogenous RhoA failed to form stress fibers (Figure 6E, indicated by black arrowheads). These results suggest that the expression of exogenous RhoA fully bypasses the requirement for BAG6 and is sufficient to rescue the stress fiber formation defects caused by BAG6 depletion. They also suggest that BAG6 might not be essential for the downstream functions of RhoA in actin fiber polymerization. Collectively, the enhanced down-regulation of endogenous RhoA protein induced by BAG6 depletion is likely a major cause of stress fiber dissociation induced by BAG6 depletion.

BAG6 knockdown enhances RhoA polyubiquitination

The stability of Rho GTPases is reported to be regulated by ubiquitination (Doye *et al.*, 2002; Chen *et al.*, 2009; Nethe and Hordijk, 2010). We confirmed that WT RhoA was constitutively polyubiquitinated in HeLa cells, whereas WT Rac1 showed relatively low levels of ubiquitination in our experimental condition (Figure 7, A and B). The polyubiquitination of WT RhoA is largely attributed to that of GDP-bound inactive RhoA species because the stability of GDP-bound RhoA (T19N) is much lower than that of the GTP-bound form (Q63L) (Supplemental Figure S5, C and D). Since a portion of RhoA is constitutively ubiquitinated (Figure 7A), we suspected that BAG6 may

FIGURE 6: BAG6 depletion makes endogenous RhoA unstable. (A) CHX chase experiments showing that endogenous RhoA is a stable protein (Control siRNA), while it becomes highly unstable following BAG6 depletion (*BAG6* siRNA). HeLa cells were transfected with siRNA duplexes for *BAG6* #1 or control. At 48 h after transfection, the cells were chased with 50 μg/ml CHX and harvested at the indicated time after CHX addition. Tubulin was used as a loading control. Efficacy of endogenous BAG6 knockdown in HeLa cells was verified by Western blot experiments. See also Supplemental Figure S5A. (B) Graphs indicate the quantified signal intensities of endogenous RhoA relative to loading controls at the indicated time points after CHX addition. The results of negative control siRNA are indicated as a blue line, and those with *BAG6* siRNA #1 are indicated with an orange line. The value of RhoA at 0 h was defined as 1.0. The graph represents the mean ± SD calculated from three independent biological replicates. $*p < 0.05$ (Student's *t* test). (C) BAG6 depletion makes exogenously expressed Flag-tagged wild-type RhoA unstable. (D) The degradation of endogenous RhoA induced by *BAG6* knockdown was blocked by proteasome inhibitors. At 72 h after siRNA transfection, HeLa cells were treated with 50 μg/ml CHX as well as 0.1% DMSO (as a negative control), 10 μM MG-132, 5 μM bortezomib, or 0.1 μM bafilomycin A1 for the indicated periods. (E) Forced expression of wild-type RhoA rescues the stress fiber formation defects in BAG6-depleted cells. At 48 h after cotransfection with siRNA duplexes (10 nM each) and a Flag-tagged RhoA expression vector (wild-type; WT), HeLa cells were stained with an anti-Flag antibody (shown as green signals) and Texas Red-labeled phalloidin (shown as red signals). Cells with exogenous RhoA expression are indicated by white arrowheads, and cells with a lack of exogenous RhoA are indicated by black arrowheads. Nuclei were stained with Hoechst 33342 (shown as blue signals). Scale bar = 10 μm.

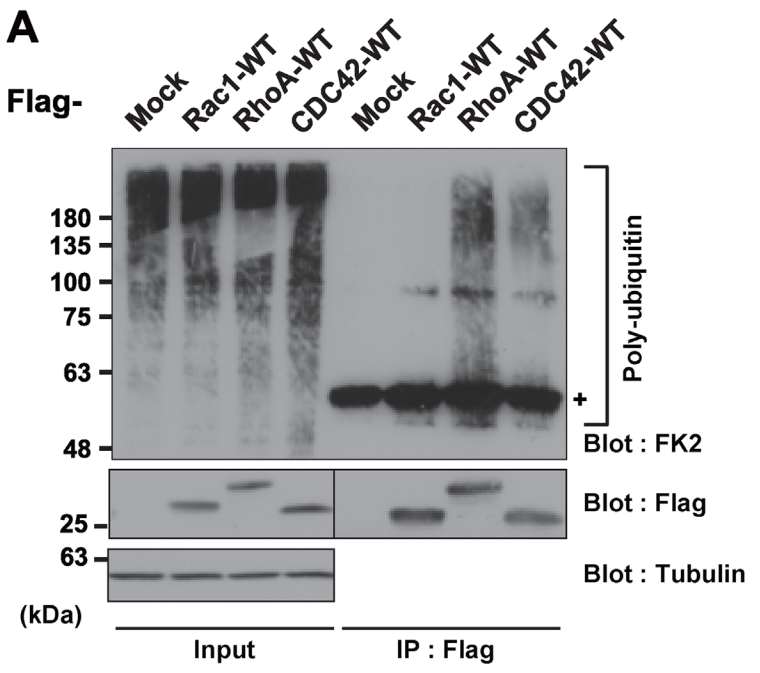
A
Flag-
Mock
Rac1-WT
RhoA-WT
CDC42-WT
Mock
Rac1-WT
RhoA-WT
CDC42-WT
180
135
100
75
63
48
25
63
(kDa)
Poly-ubiquitin
+
Blot : FK2
Blot : Flag
Blot : Tubulin
Input
IP : Flag

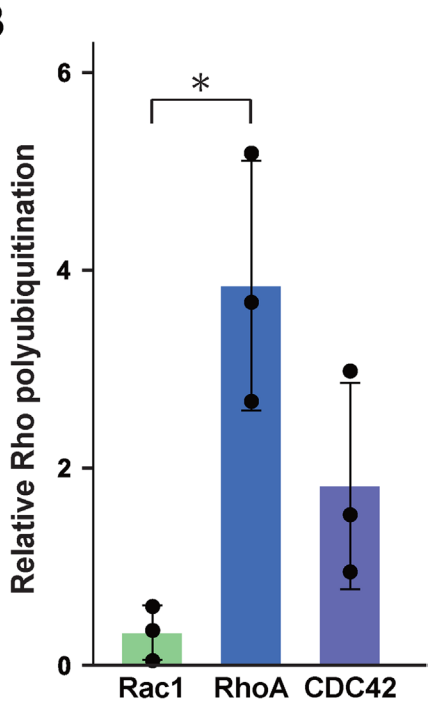
B
Relative Rho polyubiquitination
6
4
2
0
*
Rac1
RhoA
CDC42

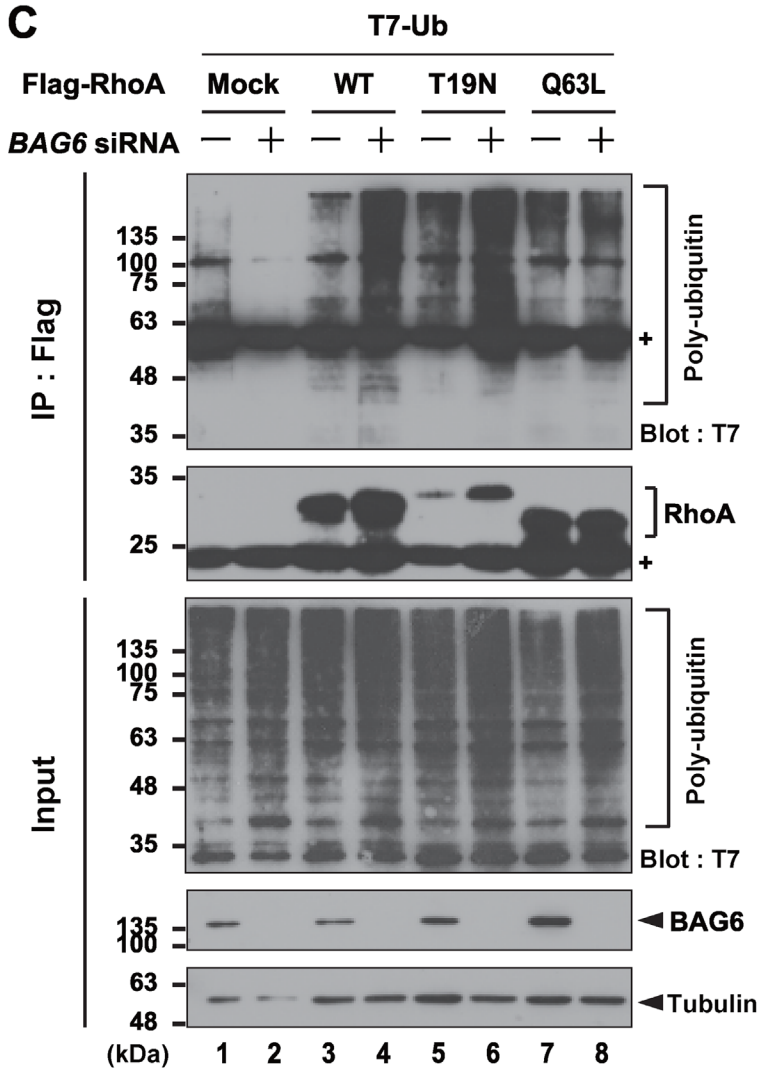
C
T7-Ub
Flag-RhoA
Mock
WT
T19N
Q63L
BAG6 siRNA
— + — + — + — +
IP : Flag
135
100
75
63
48
35
Poly-ubiquitin
+
Blot : T7
35
25
RhoA
+
Input
135
100
75
63
48
35
Poly-ubiquitin
Blot : T7
135
100
BAG6
63
48
Tubulin
(kDa)
1 2 3 4 5 6 7 8

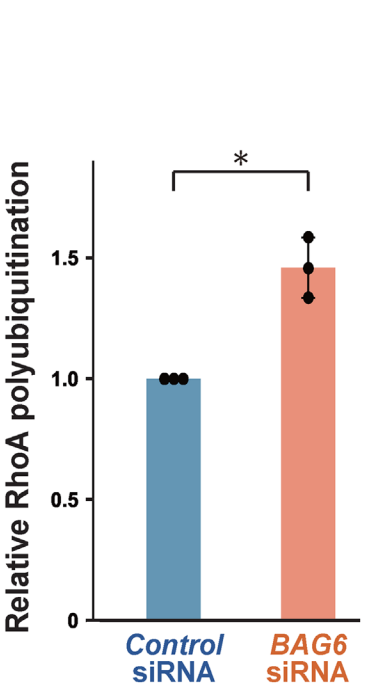
D
Relative RhoA polyubiquitination
1.5
1.0
0.5
0
*
Control siRNA
BAG6 siRNA

mediate RhoA polyubiquitination by recruiting RNF126, a BAG6-associate E3 ligase. Therefore we depleted or overexpressed RNF126 in cells and tested its effects on RhoA ubiquitination. We found that polyubiquitination of RhoA was not dependent on the levels of this E3 ligase (Supplemental Figure S6, A and B). In addition, we showed that the less ubiquitinated Rac1 is relatively stable irrespective of its nucleotide-bound status (Supplemental Figure S5, E and F).

Given that the instability of endogenous RhoA under BAG6 depletion was blocked by proteasome inhibition (Figure 6D), we hypothesized that BAG6 depletion might enhance RhoA polyubiquitination. We found that BAG6 depletion tends to stimulate the polyubiquitination of RhoA (Figure 7, C and D, see also Supplemental Figure S6, C and D), although the polyubiquitination of GTP-bound RhoA-Q63L was not severely affected (Figure 7C, compare lanes 7 and 8). These results imply that endogenous BAG6 may be necessary for blocking the proteasomal degradation of RhoA by preventing the polyubiquitination of RhoA.

BAG6 prevents the interaction of RhoA and E3 ligases to stabilize RhoA protein

Because RhoA polyubiquitination seems to be enhanced by BAG6 depletion (Figure 7C), we hypothesized that *BAG6* knockdown would stimulate the association of RhoA with ubiquitin E3 ligases. The ubiquitin ligase CUL3-complex selectively interacts with GDP-bound RhoA, rather than GTP-bound or nucleotide-free RhoA, to mediate its ubiquitination and proteasomal degradation (Chen *et al.*, 2009). We confirmed that CUL3 associated predominantly with RhoA in a nucleotide-dependent manner (Supplemental Figure S5G). We found that BAG6 depletion significantly increased the association of RhoA-T19N with CUL3 (Figure 8A, see also Supplemental Figure S7A). In the presence of MG-132, multiubiquitinated species of RhoA-T19N were detected predominantly in BAG6-depleted cells (indicated by arrowheads in Figure 8B). The enhanced association of WT RhoA with CUL3 was also obvious in BAG6-depleted cells (Figure 8B). In contrast, the coprecipitation of GTP-bound RhoA-Q63L with CUL3 was not increased by BAG6 depletion (Figure 8B). These results suggest that BAG6 inhibits the association of CUL3 with GDP-bound RhoA, thus preventing the CUL3-mediated polyubiquitination and subsequent degradation of RhoA in a nucleotide-specific manner.

Stress fiber formation defects associated with BAG6 depletion are suppressed by CUL3 knockdown

To examine whether the enhanced association of CUL3 with GDP-bound RhoA is responsible for the defects in stress fiber assembly induced by BAG6 knockdown, we codepleted CUL3 and BAG6. We confirmed that BAG6 depletion reproducibly abolished stress fiber formation (Figure 8C, compare a and b), while CUL3 depletion induced the massive formation of stress fibers (Figure 8Cc). Strikingly, codepletion of CUL3 and BAG6 induced the excess stress fiber formation phenotype (Figure 8Cd), which was indistinguishable from that of *CUL3* knockdown (Figure 8Cc). This observation suggests that codepletion of CUL3 and BAG6 fully overrides the defect in stress fiber formation induced by *BAG6* knockdown. Western blot analysis confirmed that codepletion of CUL3 and BAG6 did not compromise their respective knockdown efficiencies (Supplemental Figure S7B).

To investigate whether CUL3-based ubiquitin ligases are involved in the increased degradation of RhoA induced by BAG6 depletion, we examined the stability of endogenous RhoA under simultaneous depletion of CUL3 and BAG6. In accordance with the observation of stress fiber formation, the instability of endogenous RhoA induced by *BAG6* knockdown was almost completely suppressed by CUL3 depletion (Figure 8D). These observations suggest that BAG6 protects RhoA from degradation by inhibiting its access to CUL3-based ubiquitin ligases. Eventually, this mechanism should support the appropriate formation of stress fibers.

RhoA ubiquitination is determined by a specific region including Switch I

Rac1 is a stable protein with no detectable affinity for BAG6 (Figure 1, A and B and Supplemental Figure S5, E and F), whereas BAG6 possesses an affinity for RhoA and plays a critical role in its stability (Figures 1A and 6, A–D), even though these small GTPases share high overall amino acid sequence similarity (69% identity and 78% similarity). To address the mechanism of the BAG6-mediated inhibition of RhoA ubiquitination, we prepared a series of RhoA-Rac1 chimeric proteins (Figure 9A). We found that a RhoA-Rac1 chimera with the N-terminal 57 residues of RhoA (designated as the N57 chimera) was very unstable (Figure 9, A and B), whereas a RhoA-Rac1 chimera with the N-terminal 23 residues of RhoA (designated as the N23 chimera) showed enhanced stability even in its GDP-bound form (Figure 9, A and B). In accordance with these observations, the N57 chimera was found to be polyubiquitinated, while the N23 chimera was not (Figure 9, C and D). These observations suggest that a small region of RhoA (from residues 24 to 57), which includes the Switch I loop of the GTPase domain (Supplemental Figure S8, A and B), is critical for the instability and polyubiquitination of RhoA in a GDP-bound form-specific manner.

FIGURE 7: BAG6 knockdown enhances RhoA polyubiquitination. (A, B) Wild-type RhoA protein is constitutively polyubiquitinated, while Rac1 is not. A series of Flag-tagged wild-type Rho family GTPases, Rac1, RhoA, and CDC42 were immunoprecipitated from HeLa cell extracts and probed with an anti-polyubiquitin FK2 antibody to detect their potential polyubiquitination. Note that all cells were treated with 10 μM MG-132 for 4 h before harvest. A plus mark (+) indicates an immunoglobulin heavy chain band. The graph in B shows the relative signal intensities of coprecipitated polyubiquitin with Rho-family small GTPases (signal intensities of the FK2 blots were divided by those of the Flag blots). $*p < 0.05$ (Student's *t* test). (C, D) Polyubiquitination of RhoA seems to be enhanced by BAG6 depletion. Flag-tagged RhoA in its WT, GDP-bound (T19N), and GTP-bound (Q63L) forms was immunoprecipitated from BAG6-depleted (+) or control (–) cell extracts and blotted with an anti-T7-ubiquitin antibody. BAG6 siRNA duplex #1 was used. Note that all cells were treated with 10 μM MG-132 for 4 h before harvest, thus RhoA proteins were stabilized even in the presence of BAG6 siRNA (C). Plus marks (+) indicate immunoglobulin heavy or light chains. See also Supplemental Figure S6, C and D for replicated experiments. The graph in D shows the relative signal intensities of coprecipitated polyubiquitin with wild-type RhoA (signal intensities of the T7 ubiquitin blots were divided by those of the Flag blots). $*p < 0.05$ (Student's *t* test).

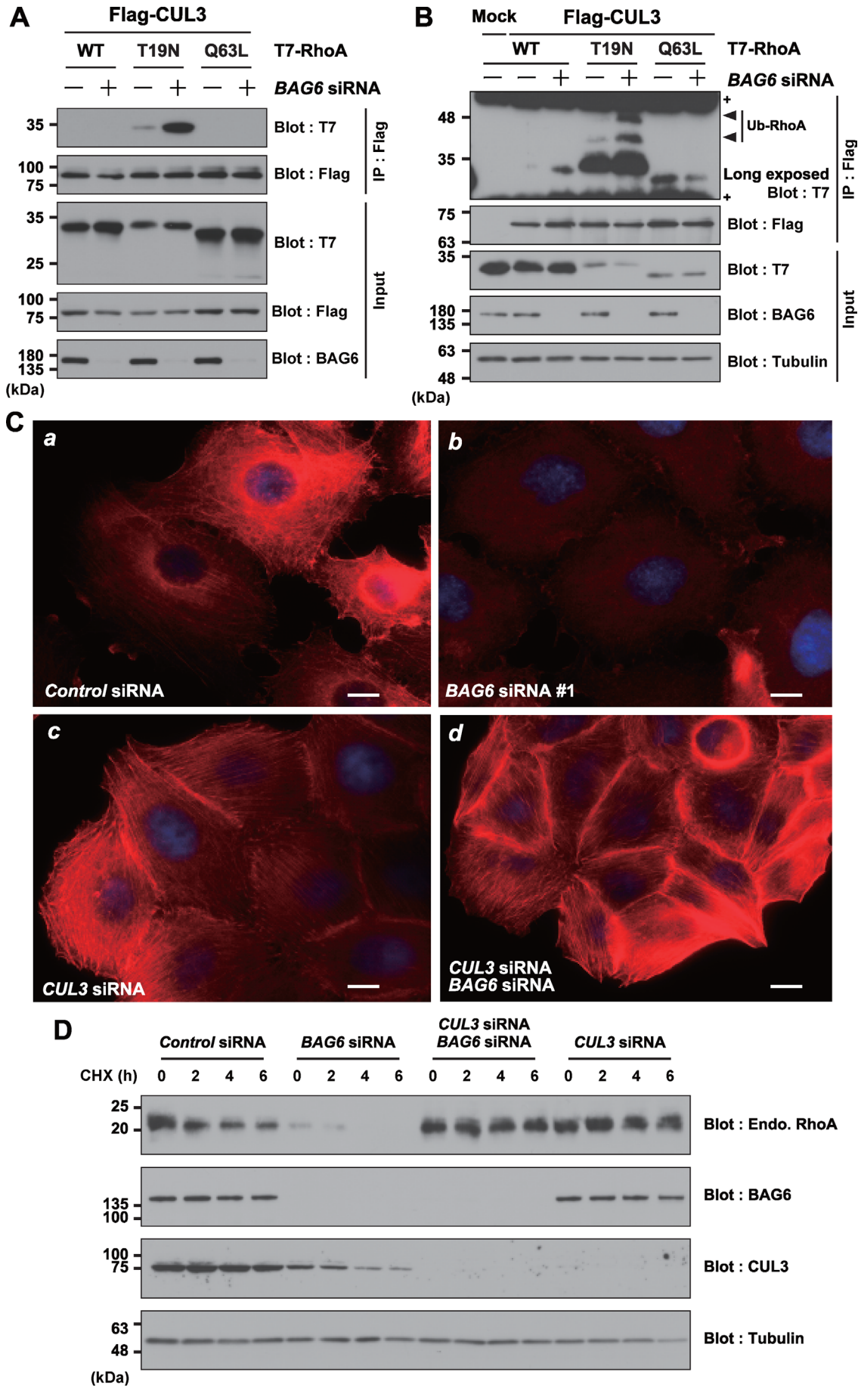
A
Flag-CUL3
WT
T19N
Q63L
T7-RhoA
BAG6 siRNA
35
100
75
Blot : T7
Blot : Flag
IP : Flag
35
25
Blot : T7
100
75
Blot : Flag
Input
180
135
Blot : BAG6
(kDa)
B
Mock
Flag-CUL3
WT
T19N
Q63L
T7-RhoA
BAG6 siRNA
48
35
Ub-RhoA
Long exposed
Blot : T7
IP : Flag
75
63
Blot : Flag
35
Blot : T7
Input
180
135
Blot : BAG6
63
48
Blot : Tubulin
(kDa)
C
a
Control siRNA
b
BAG6 siRNA #1
c
CUL3 siRNA
d
CUL3 siRNA
BAG6 siRNA
D
Control siRNA
BAG6 siRNA
CUL3 siRNA
BAG6 siRNA
CUL3 siRNA
CHX (h)
0 2 4 6 0 2 4 6 0 2 4 6 0 2 4 6
25
20
Blot : Endo. RhoA
135
100
Blot : BAG6
100
75
Blot : CUL3
63
48
Blot : Tubulin
(kDa)

BAG6 inhibits the association of CUL3 and RhoA by competing for a common region

As a small region of RhoA (residues 24 to 57) was found to be critical for its polyubiquitination (Figure 9, C and D), we hypothesized that BAG6 and CUL3-based ubiquitin ligases might recognize an overlapping region of RhoA to modulate its stability. Therefore we examined whether BAG6 and CUL3 coprecipitated with the chimeric RhoA proteins. We found that the RhoA-Rac1 N57 chimera showed affinity for CUL3, while the N23 chimera lost its affinity for CUL3 (Figure 9, E and G, note that the signal intensities of Flag-tagged precipitates of the N57 chimera were much weaker than those of the N23 chimera). Similarly, BAG6 associated more strongly with the N57 chimera compared with the N23 chimera (Figure 9, F and H). These results suggest that BAG6 and CUL3-based ubiquitin ligases recognize a common (or neighboring) region of GDP-bound RhoA. In accordance with this view, BAG6 depletion increased the association of the RhoA-Rac1 N57 chimera with CUL3 (Figure 9E, compare lanes 2 and 3) as was the case for RhoA (Figure 8, A and B, see also Supplemental Figure S7A), whereas the coprecipitation of CUL3 with the residual amount of RhoA-Rac1 N23 chimera showed a weak dependency on BAG6 (Figure 9E, compare lanes 4 and 5). These results imply that BAG6 and CUL3-based ubiquitin ligases likely associate with RhoA at an overlapping region between N24-57 in a competitive manner.

DISCUSSION

In this study, we found that BAG6 regulated stress fiber formation by stabilizing endogenous RhoA, a key Rho family protein in F-actin polymerization. BAG6 deficiency enhanced the association between CUL3 and RhoA (Figure 8, A and B), promoted its polyubiquitination (Figure 7C), and stimulated the rapid proteasomal degradation of RhoA (Figure 6, A–D), leading to the abrogation of F-actin polymerization (Figure 2). The restoration of RhoA expression rescued stress fiber formation defects (Figure 6E), bypassing the requirement for BAG6. These findings reveal a crucial role for BAG6 in actin fiber polymerization and establish BAG6 as a RhoA-stabilizing holdase that binds to and supports the function of endogenous RhoA (Figure 10).

Previous studies have revealed that BAG6 stimulates protein degradation events for protein quality control (Minami *et al.*, 2010; Hessa *et al.*, 2011; Xu *et al.*, 2013; Rodrigo-Brenni *et al.*, 2014; Suzuki and Kawahara, 2016; Guna and Hegde, 2018). BAG6 is also necessary for protein biogenesis, especially for tail-anchored transmembrane proteins (Mariappan *et al.*, 2010; Leznicki *et al.*, 2010; Kawahara *et al.*, 2013; Lee and Ye, 2013). In this study, we found a third functional category for BAG6: supporting the stability and function of RhoA. The association of BAG6 with RhoA prevents the access of E3 ubiquitin ligases to RhoA, thus inhibiting its polyubiquitination for proteasomal degradation. This is a unique function of BAG6 that is independent of its previously suggested role in stimulating the degradation of Rab family proteins and newly synthesized defective proteins. In accordance with this view, the depletion of BAG6-associated components for protein degradation, such as proteasomal ubiquitin receptor UBQLN4 and BAG6-associated E3 ligase RNF126, did not affect stress fiber formation (Figure 3). It is also possible that ubiquitinated RhoA on BAG6 could be deubiquitinated immediately in the cytosol for stabilization, as suggested by a recent study showing that ubiquitinated tail-anchored proteins can be deubiquitinated and their functions are rescued by USP20 and USP33 (Culver and Mariappan, 2021).

Even though RhoA and Rab8a belong to the common small GTPase family, it is interesting to note that BAG6 exerted quite opposite effects on RhoA and Rab8a. Indeed, BAG6 was shown to be necessary for the degradation of Rab8a in its GDP-bound form (Takahashi *et al.*, 2019), while we found that BAG6 was critical for the stabilization of GDP-bound RhoA. How BAG6 determines the different fates of similar GTPases, RhoA for stabilization and Rab8a for degradation, is a critical question for further study. In the case of Rab8a, RABIF/MSS4 was suggested to function as a holdase for the nucleotide-free forms of a subset of Rab proteins (Gulbranson *et al.*, 2017). In mammalian cells lacking RABIF, newly synthesized Rab8a protein is degraded rapidly. In addition to Rab8a, the expression of Rab10 and Rab13 is also reduced in RABIF-depleted cells, whereas the expression of other Rabs is not significantly affected (Gulbranson *et al.*, 2017), suggesting that RABIF stabilizes a limited number of Rab family proteins. Similarly, BAG6 is necessary for endogenous RhoA stabilization, while the stability of Rac1, a closely related Rho family protein, was independent of the presence of BAG6.

Rac1 degradation is reported to occur during the onset of epithelial-mesenchymal transition, resulting in the transient and local inactivation of this Rho family protein (Lynch *et al.*, 2006). RhoA is polyubiquitinated by another E3 ligase, Smurf1, which also stimulates the local down-regulation of RhoA at the leading edge (specific cellular protrusion) to promote cell motility (Doye *et al.*, 2002; Wang *et al.*, 2003; Sahai *et al.*, 2007). Such Smurf1-mediated local elimination was proposed to be specific for the active GTP-bound species of RhoA (Doye *et al.*, 2002; Boyer *et al.*, 2006; Sahai *et al.*, 2007), making a clear contrast to the CUL3-mediated polyubiquitination machinery whose RhoA-specific substrate receptor BACURD possesses a preference for GDP-bound RhoA (Chen *et al.*, 2009).

FIGURE 8: BAG6 prevents the physical interaction of CUL3 and RhoA. (A, B) The interaction between CUL3 and RhoA is stimulated by BAG6 depletion either in the absence (A) or presence (B) of MG-132. Cells were treated with (+) or without (–) 10 nM *BAG6* siRNA duplex #1 for 48 h. In the presence of MG-132, ubiquitin-modified RhoA-T19N bands (indicated by arrowheads) were strengthened in BAG6-depleted cells (B). Note that the T7 blot in (B) was overexposed. Coprecipitation of WT RhoA with CUL3 can also be detected in BAG6-depleted cells (B). Plus marks (+) indicate immunoglobulin heavy or light chains. See also Supplemental Figure S7A. (C) Defects in stress fiber formation induced by BAG6 depletion are suppressed by *CUL3* knockdown. At 48 h after transfection with 10 nM siRNA duplexes for control (a), *BAG6* (b), and *CUL3* (c). CUL3 and BAG6 were simultaneously depleted with their siRNA duplexes (5 nM each) (d). HeLa cells were stained with Texas Red-labeled phalloidin (shown as red signals). Note that all images presented in this figure were acquired in an identical set of experiments, and the exposure time of all photographs was the identical. Nuclei were stained with Hoechst 33342 (shown as blue signals). Scale bar: 10 μm. See also Supplemental Figure S7B. (D) RhoA degradation induced by BAG6 knockdown is suppressed by CUL3 depletion. At 48 h after transfection with siRNA duplexes (total 10 nM) for control, *BAG6*, *CUL3*, and a mixture of *CUL3/BAG6*, HeLa cells were chased with 50 μg/ml CHX and harvested at the indicated time after CHX addition. Knockdown efficacies were verified by Western blot analyses with respective antibodies. Tubulin was used as a loading control.

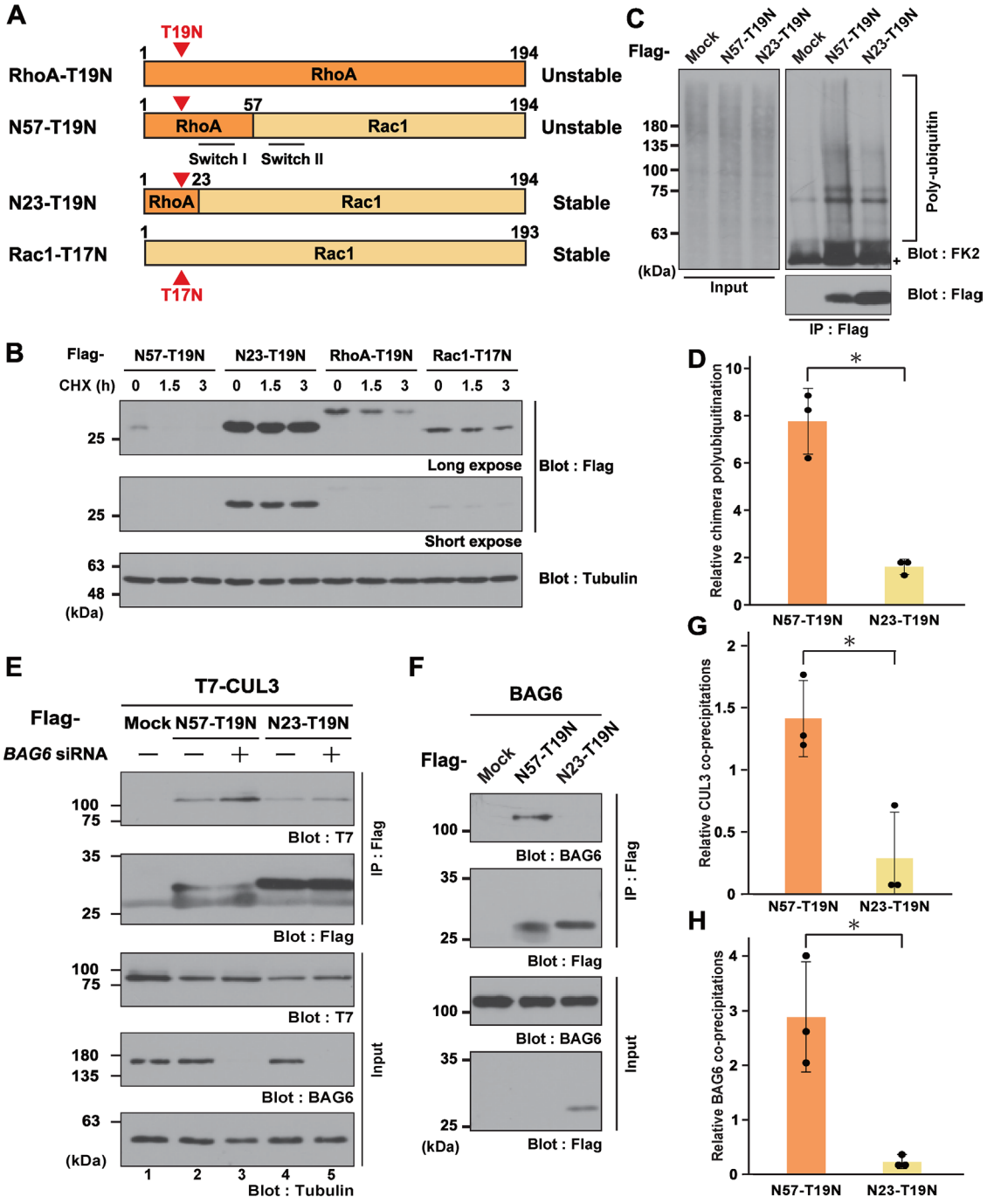

FIGURE 9: RhoA ubiquitination is determined by a specific region including Switch I. (A) Schematic of the RhoA-Rac1 chimeric proteins used in this study. Note that all the chimeric proteins possess the T19N GDP-bound mutation. The RhoA-Rac1 N57 chimera includes the Switch I region of RhoA, while the N23 chimera possesses the Switch I region of Rac1. See also Supplemental Figure S8. (B) CHX chase experiments showing that the RhoA-Rac1 N57 chimera is a labile protein, while the N23 chimera is highly stable in HeLa cells. The chimeric proteins were expressed in HeLa cells and then chased with 50 μg/ml CHX for the indicated periods. Tubulin was used as a loading control. (C, D) The RhoA-Rac1 N57 chimera is polyubiquitinated, while the N23 chimera is not. Flag-tagged chimera proteins were immunoprecipitated from the extracts of MG-132-treated HeLa cells and blotted with an anti-polyubiquitin FK2 antibody (C). A plus mark (+) indicates immunoglobulin heavy chain bands. Coprecipitated polyubiquitin signals were quantified (D). Note that the signal intensities of polyubiquitin were normalized using the coprecipitated Flag signals. *$p < 0.05$ (Student's *t* test). (E, G) CUL3 coprecipitates with the RhoA-Rac1 N57 chimera, while the N23 chimera coprecipitates with only a small amount of CUL3 (E). Note that all cells were treated with 10 μM MG-132 for 4 h before harvest. Coprecipitated signals of CUL3 with RhoA-Rac1 chimeras were quantified (G). Note that the signal intensities of CUL3 were normalized using the coprecipitated Flag signals. The graph represents the mean ± SD calculated from three independent biological replicates. *$p < 0.05$ (Student's *t* test). (F, H) BAG6 coprecipitates with the RhoA-Rac1 N57 chimera, but not with the N23 chimera (F). Coprecipitated BAG6 signals were quantified (H). Note that the signal intensities of BAG6 were normalized using the coprecipitated Flag signals. *$p < 0.05$ (Student's *t* test).

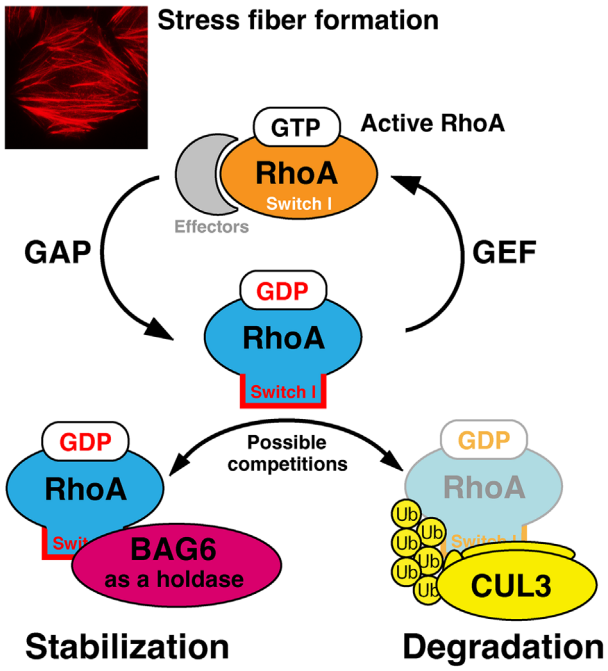

FIGURE 10: Summary of this study. BAG6 protects RhoA from ubiquitin-dependent degradation to support stress fiber formation.

CUL3-BACURD ubiquitin ligase seems to be involved in not only the local degradation of RhoA but also its global elimination. Similarly, BAG6 depletion stimulates global defects in stress fiber formation and RhoA stability.

Both CUL3 and BAG6 possess a preference for GDP-bound RhoA, suggesting that BAG6 and CUL3-BACURD ubiquitin ligase recognize a common target sequence. Although RhoA and Rac1 share high overall similarity in their primary structure, BAG6 recognizes GDP-bound RhoA far stronger than that for Rac1 (Figure 1), implying that sequence differences of RhoA and Rac1 should determine their respective stability and BAG6 dependency. Indeed, this study revealed that the region around Switch I (from ^{24}Val to ^{57}Leu of human RhoA) is necessary for its interactions with BAG6 and CUL3 because the RhoA-Rac1 N57 and N23 chimeras showed a clear difference in their affinity for CUL3 and BAG6, as well as BAG6 dependency for their stability. Furthermore, the Switch I region is known to change its tertiary structure depending on the nucleotide-binding status (Supplemental Figure S8). Therefore the region from ^{24}Val to ^{57}Leu of RhoA might determine the ubiquitination efficiency of RhoA in a GDP-bound form-specific manner. The Switch I region contains several RhoA-specific hydrophobic residues (Supplemental Figure S8A) that might be critical for the instability of GDP-bound RhoA. In accordance with this view, our preliminary analysis suggests that substitutions of the hydrophobic residues (such as ^{33}Val) in the Switch I region make GDP-bound RhoA highly stable. In addition, this region does not appear to overlap fully with the binding face for ARHGEF2, a guanine nucleotide exchange factor for RhoA (PDB 8BNT, Supplemental Figure S9), although this point should be examined further by additional study.

An important issue that remains to be elucidated is the physiological relevance of the BAG6-mediated inhibition of CUL3-RhoA interactions. Because the N-terminus of BAG6 is necessary for the recognition of defective proteins that accumulate in stressed cells (Minami *et al.*, 2010; Hessa *et al.*, 2011; Guna and Hegde, 2018), we speculate that BAG6 might be a kind of stress sensor that can modulate the stability of RhoA in a stress-dependent manner. RhoA-controlled actin cytoskeleton dynamics determine the potential for cell migration and provide a driving force for cell movement, including in cancer metastasis and invasion (Sahai and Marshall, 2002; Vega and Ridley, 2008; Haga and Ridley, 2016). Therefore investigating the modifications of RhoA stability induced by tumor-associated stress might be an interesting challenge for future study.

MATERIAL AND METHODS

Request a protocol through *Bio-protocol*.

Mammalian cell culture and transfection

Human immortal epithelial cell line HeLa was cultured in D-MEM (Fuji-Wako, Japan) supplemented with 5% heat-inactivated fetal bovine serum (FBS) at 37°C under 5% CO_2 atmosphere. Human neuroblastoma SH-SY5Y cells were cultured in D-MEM/Ham's F12 medium (Fuji-Wako) supplemented with 10% heat-inactivated FBS at 37°C under 5% CO_2 atmosphere. Human breast cancer cell line MDA-MB-231 (JCRB) was cultured in D-MEM (Fuji-Wako) supplemented with 10% heat-inactivated FBS at 37°C under 5% CO_2 atmosphere.

Transfections of the expression vectors were performed with HilyMax (Dojindo, Japan) or polyethylenimine "Max" transfection reagent (Polysciences, Inc.) according to the protocols supplied by the manufacturers. At 18–24 h after transfection, the cells were harvested and subjected to immunological analysis unless otherwise noted.

RNA interference

BAG6 depletions in HeLa and cells were performed as described previously (Minami *et al.*, 2010) with three independent duplex siRNAs covering the targeted sequences:

5′-UUUCUCCAAGAGCAGUUUAdtdt-3′ (*BAG6* siRNA#1),

5′-ACCGGAAUGCCAACAGCUAdtdt-3′ (*BAG6* siRNA#6),

5′-AGGAGGAUCAGCGGUUGATdtdt-3′ (*BAG6* siRNA#8).

The siRNA target sequences specific for *CUL3*, *UBQLN4*, *RNF126*, *RNF115*, and *UBL4A* were synthesized as below:

5′-CAAAUAAAAGUGUUUCUGAdtdt-3′ (*CUL3* siRNA)

5′-CAAACAGCAGGGUGACUUUdtdt-3′ (*UBQLN4* siRNA)

5′-CAUCCCGGACGGUACUUCUdtdt-3′ (*RNF126* siRNA)

5′-CUUGCAAUCACUUCUUUCAdtdt-3′ (*RNF115* siRNA)

5′-UCUGGCAGCUGAUCUCCAAdtdt-3′ (*UBL4A* siRNA).

AllStars Negative Control siRNA (QIAGEN) or MISSION siRNA Universal Negative Control 1 (Sigma-Aldrich) was used as general negative control in each experiment. We also designed scrambled siRNA for BAG6 siRNA#1 as a negative control for BAG6 knockdown experiments in human cells as follows:

5′-UCUGCAAAUGUCCUUUAAGdtdt-3′(BAG6 siRNA#1 scr).

Transfections of duplex siRNAs to human cultured cells were performed using Lipofectamine RNAiMAX (Invitrogen) or Lipofectamine 2000 (Invitrogen) according to the protocols provided by the manufacturer. The efficacy of each siRNA was verified by immunoblot with their specific antibodies listed in following section.

Plasmid construction

Full-length cDNAs of human RhoA, Rac1, CDC42, and RhoC were amplified by PCR from cDNA library derived from SH-SY5Y cells.

The PCR fragments were cloned into pCI-neo-based mammalian expression vectors (Promega) with N-terminal 3 × Flag-tags or N-terminal 3 × T7-tags with their products. GDP-bound and GTP-bound mutants were prepared by inverse PCR. Vectors were used for experiments after verification of the sequence of inserted DNA. Expression vectors for 2× S-tags-BAG6 (Takahashi *et al.*, 2019), 3× T7-CUL3 (Noguchi *et al.*, 2018), 3× Flag-BAG6 N465, and ΔN465 (Hayashishita *et al.*, 2019) were described previously. Genes encoding RhoA-Rac1 chimeric proteins (chimeras N57 and N23) were chemically synthesized (Eurofins Genomics Inc., Japan) and subcloned into pCI-neo-based mammalian expression vectors.

Immunological analysis

For immunoprecipitation (IP) analysis, HeLa cells were washed with ice-cold phosphate-buffered saline (PBS) and lysed with IP buffer containing 20 mM Tris-HCl, pH 7.5, 150 mM NaCl, 5 mM EDTA, 1% NP-40, 25 μM MG-132, 10 mM NEM, and protease inhibitor cocktail (Nacalai tesque). The lysates were pipetted, centrifuged at 15,000 rpm for 10–20 min at 4 °C, and mixed with 5–10 μl of anti-Flag M2 affinity gel (Sigma) for 15 min-2 h at 4°C. After the beads had been washed five times with the IP buffer, the immunocomplexes were eluted by SDS sample buffer.

For Western blot analyses, whole cell lysates or the immunoprecipitates were subjected to SDS–PAGE and transferred onto polyvinylidene fluoride transfer membrane (GE Healthcare, Pall Corporation). The membranes were then immunoblotted with specific primary antibodies as indicated and then incubated with horseradish peroxidase–conjugated antibody against mouse or rabbit immunoglobulin (GE Healthcare), followed by detection with ECL Western blotting detection reagents (GE Healthcare) or Clarity Western ECL substrate (Bio-Rad).

The following antibodies were used in this study: anti-RhoA (Cytoskeleton #ARH04, Abcam ab54835), anti-CUL3 (Cell Signaling Technology #2759), anti-Rac1 23A8 (Abcam ab33186), anti-Paxillin Y113 (Abcam ab32084), anti-BAG6 (Minami *et al.*, 2010), anti-Flag M2 monoclonal (Sigma F1804), anti-Flag polyclonal (Sigma F7425), anti-T7-tag monoclonal (Novagen 69522), anti-α-tubulin monoclonal (Sigma T6199), and anti-polyubiquitin FK2 (MBL D058-3).

Microscopic observations

For cytochemical observations, HeLa cells that were grown on micro cover glass (Matsunami) were washed twice with PBS, fixed by incubating in 4% paraformaldehyde for 10 min, and permeabilized with 0.1% Triton X-100 for 3 min at room temperature. Fixed cells were blocked with 3% heat-inactivated FBS in PBS and then reacted with a Texas Red-X phalloidin (Invitrogen). For nuclear observations, cells were stained with Hoechst 33342. Cells reacted with anti-Paxillin antibody were incubated at 4°C for overnight and were subsequently reacted with Alexa Fluor^{R}-488 anti-rabbit IgG as a secondary antibody. Immunofluorescence images were obtained with BIOREVO BZ9000 fluorescence microscope (Keyence, Japan).

Flow cytometry

HeLa cells on 100-mm dishes were trypsinized, pipetted with growth medium, and centrifuged at 1000 rpm for 3 min. The cell pellets were washed once in PBS, resuspended in 500 μl 70% ethanol, and incubated for 30 min at –20°C. After fixation, the cells were precipitated and washed twice in 1% bovine serum albumin (BSA)/PBS. For actin stress fiber staining, the cells were resuspended in 300 μl solution containing phalloidin-iFluor 488 Reagent (Abcam, 1/50,000 dilution) in PBS containing 0.4% Triton X-100, and incubated for 1 h at 4°C. The cells were washed twice in 1% BSA/PBS. Flow cytometry analyses were performed by BD Accuri C6 flowcytometer (Becton Dickinson). Data from populations of 50,000 cells were analyzed using BD Accuri C6 software. Statistical significance was calculated based on three independent biological replicates.

Wound-healing assay

HeLa cells were grown to 80% confluence in the 35-mm dishes after transfection of siRNAs for 2 d. After mitomycin C treatment (3 μg/ml for 1 h), cell layers were scratched vertically with a small pipette tip and washed with PBS to remove cells. Subsequently, cell dishes were supplemented with fresh medium and continued to grow for 24 h. Photographs were taken to observe and measure the cell migration quantitatively.

Video microscopy and single-cell tracking assay

MDA-MB-231 cells were seeded in collagen-coated glass-bottomed 35-mm dishes. Each dish was placed in a stage top incubator on a BZ-X700 All-in-One Microscope (Keyence). The cells were automatically imaged at multiple positions per dish using a phase contrast 40× objective lens (Nikon) for 8 h with 10-min intervals. In each experiment, four fields were simultaneously recorded using an automated stage. Tracking analysis was performed by the "MTrackJ" and "Chemotaxis and Migration Tool" plug-in for ImageJ with generation of Wind-Rose plots and determination of the migration parameters "accumulated distance" and "Euclidean distance" (Blockhuys *et al.*, 2020).

Statistics

Statistical analyses were performed using a Student's *t* test, if not stated otherwise, and quantified data are presented as mean ± SD as indicated in figure legends. All experiments were performed at least three independent biological replicates to compute statistical significance. A $p < 0.05$ was considered statistically significant.

ACKNOWLEDGMENTS

We thank Naoto Yokota, Toshiki Takahashi, Yasuyuki Iwasa, Taro Saito, and Akiko Asada (Tokyo Metropolitan University) for valuable suggestions and technical assistance. This work was supported in part by grants from the Japan Society for the Promotion of Science (JSPS) KAKENHI (Chemo-Ubiquitin, No. 19H05293 and No. 20H00457), the Takeda Science Foundation and Research fund for future infectious disease measures from Tokyo Metropolitan Government to H.K.

REFERENCES

Anne R (2015). Rho GTPase signalling in cell migration. Curr Opinion Cell Biol 36, 103–112.

Bishop AL, Hall A (2000). Rho GTPases and their effector proteins. Biochem J 348, 241–255.

Blockhuys S, Zhang X, Wittung-Stafshede P (2020). Single-cell tracking demonstrates copper chaperone Atox1 to be required for breast cancer cell migration. Proc Natl Acad Sci USA 117, 2014–2019.

Boyer L, Turchi L, Desnues B, Doye A, Ponzio G, Mege JL, Yamashita M, Zhang YE, Bertoglio J, Flatau G, *et al.* (2006). CNF1-induced ubiquitylation and proteasome destruction of activated RhoA is impaired in Smurf1-/- cells. Mol Biol Cell 17, 2489–2497.

Bryan B, Cai Y, Wrighton K, Wu G, Feng XH, Lie M (2005). Ubiquitination of RhoA by Smurf1 promotes neurite outgrowth. FEBS Lett 579, 1015–1019.

Chen Y, Yang Z, Meng M, Zhao Y, Dong N, Yan H, Liu L, Ding M, Peng HB, Shao F (2009). Cullin mediates degradation of RhoA through evolutionarily conserved BTB adaptors to control actin cytoskeleton structure and cell movement. Mol Cell 35, 841–855.

Culver JA, Mariappan M (2021). Deubiquitinases USP20/33 promote the biogenesis of tail-anchored membrane proteins. J Cell Biol 220, e202004086.

Ding F, Yin Z, Wang HR (2011). Ubiquitination in Rho signaling. Curr Top Med Chem 11, 2879–2887.
Doye A, Mettouchi A, Bossis G, Clément R, Buisson-Touati C, Flatau G, Gagnoux L, Piechaczyk M, Boquet P, Lemichez E (2002). CNF1 exploits the ubiquitin-proteasome machinery to restrict Rho GTPase activation for bacterial host cell invasion. Cell 111, 553–564.
Dupraz S, Hilton BJ, Husch A, Santos TE, Coles CH, Stern S, Brakebusch C, Bradke F (2019). RhoA controls axon extension independent of specification in the developing brain. Curr Biol 29, 3874–3886.e9.
Etienne-Manneville S, Hall A (2002). Rho GTPases in cell biology. Nature 420, 629–635
Fonseca AV, Freund D, Bornhäuser M, Corbeil D (2010). Polarization and migration of hematopoietic stem and progenitor cells rely on the RhoA/ROCK I pathway and an active reorganization of the microtubule network. J Biol Chem 285, 31661–31671.
Genau HM, Huber J, Baschieri F, Akutsu M, Dötsch V, Farhan H, Rogov V, Behrends C (2015). CUL3-KBTBD6/KBTBD7 ubiquitin ligase cooperates with GABARAP proteins to spatially restrict TIAM1-RAC1 signaling. Mol Cell 57, 995–1010.
Gulbranson DR, Davis EM, Demmitt BA, Ouyang Y, Ye Y, Yu H, Shen J (2017). RABIF/MSS4 is a Rab-stabilizing holdase chaperone required for GLUT4 exocytosis. Proc Natl Acad Sci USA 114, E8224–E8233.
Guna A, Hegde RS (2018). Transmembrane domain recognition during membrane protein biogenesis and quality control. Curr Biol 28, R498–R511.
Haga RB, Ridley AJ (2016). Rho GTPases: Regulation and roles in cancer cell biology. Small GTPases 7, 207–221.
Hall A (1998). Rho GTPases and the actin cytoskeleton. Science 279, 509–514.
Hayashishita M, Kawahara H, Yokota N (2019). BAG6 deficiency induces mis-distribution of mitochondrial clusters under depolarization. FEBS Open Bio 9, 1281–1291.
Heasman SJ, Ridley AJ (2008). Mammalian Rho GTPases: new insights into their functions from in vivo studies. Nat Rev Mol Cell Biol 9, 690–701.
Hessa T, Sharma A, Mariappan M, Eshleman HD, Gutierrez E, Hegde RS (2011). Protein targeting and degradation pathway are coupled for elimination of misfolded proteins. Nature 475, 394–397.
Jaffe AB, Hall A (2005). Rho GTPases: biochemistry and biology. Annu Rev Cell Dev Biol 21, 247–269.
Kamikubo K, Kato H, Kioka H, Yamazaki S, Tsukamoto O, Nishida Y, Asano Y, Imamura H, Kawahara H, Shintani Y, Takashima S (2019). A molecular triage process mediated by RING finger protein 126 and BCL2-associated athanogene 6 regulates degradation of G0/G1 switch gene 2. J Biol Chem 294, 14562–14573.
Kaudeer J, Koch J (2014). BAG-6, a jack of all trades in health and disease. Cell Mol Life Sci 10.1007/s00018-013-1522-y
Kawahara H, Minami R, Yokota N (2013). BAG6/BAT3; emerging roles in quality control for nascent polypeptides. J Biochem 153, 147–160.
Kikukawa Y, Minami R, Shimada M, Kobayashi M, Tanaka K, Yokosawa H, Kawahara H (2005). Unique proteasome subunit Xrpn10c is a specific receptor for the antiapoptotic ubiquitin-like protein Scythe. FEBS J 272, 6373–6386.
Kopitar AN, Markelj G, Oražem M, Blazina Š, Avčin T, Ihan A, Debeljak M (2019). Flow cytometric determination of actin polymerization in peripheral blood leukocytes effectively discriminate patients with homozygous mutation in ARPC1B from asymptomatic carriers and normal controls. Front Immunol 10, 1632.
Kovačevi I, Sakaue T, Majoleé J, Pronk MC, Maekawa M, Geerts D, Fernandez-Borja M, Higashiyama S, Hordijk PL (2018). The Cullin-3–Rbx1–KCTD10 complex controls endothelial barrier function via K63 ubiquitination of RhoB. J Cell Biol 217, 1015–1032.
Kuwabara N, Minami R, Yokota N, Matsumoto H, Senda T, Kawahara H, Kato R (2015). Structure of a BAG6 (bcl-2-associated athanogene 6)–Ubl4a (ubiquitin-like protein 4a) complex reveals a novel binding interface that functions in tail-anchored protein biogenesis. J Biol Chem 290, 9387–9398.
Lebowitz PF, Davide JP, Prendergast GC (1995). Evidence that farnesyltransferase inhibitors suppress Ras transformation by interfering with Rho activity. Mol Cell Biol 15, 6613–6622.
Lee JG, Ye Y (2013). Bag6/Bat3/Scythe: A novel chaperone activity with diverse regulatory functions in protein biogenesis and degradation. Bioessays 35, 377–385.
Leznicki P, Clancy A, Schwappach B, High S (2010). Bat3 promotes the membrane integration of tail-anchored proteins. J Cell Sci 123, 2170–2178.
Lin MC, Yu CJ, Lee FS (2022). Phosphorylation of Arl4A/D promotes their binding by the HYPK chaperone for their stable recruitment to the plasma membrane. Proc Natl Acad Sci USA 119, e2207414119.
Lynch EA, Stall J, Schmidt G, Chavrier P, D'Souza-Schorey C (2006). Proteasome-mediated degradation of Rac1-GTP during epithelial cell scattering. Mol Biol Cell 17, 2236–2242.
Maeda M, Hasegawa H, Hyodo T, Ito S, Asano E, Yuang H, Funasaka K, Shimokata K, Hasegawa Y, Hamaguchi M, Senga T (2011). ARHGAP18, a GTPase-activating protein for RhoA, controls cell shape, spreading, and motility. Mol Biol Cell 22, 3840–3852.
Mariappan M, Li X, Stefanovic S, Sharma A, Mateja A, Keenan RJ, Hegde RS (2010). A ribosome-associating factor chaperones tail-anchored membrane proteins. Nature 466, 1120–1124.
Minami R, Hayakawa A, Kagawa H, Yanagi Y, Yokosawa H, Kawahara H (2010). BAG6 is essential for selective elimination of defective proteasomal substrates. J Cell Biol 190, 637–650.
Nethe M, Hordijk PL (2010). The role of ubiquitylation and degradation in RhoGTPase signalling. J Cell Sci 123, 4011–4018.
Nobes CD, Hall A (1995). Rho, Rac, and cdc42 GTPases regulate the assembly of multimolecular focal complexes associated with actin stress fibers, lamellipodia, and filopodia. Cell 81, 53–62.
Noguchi A, Adachi S, Yokota N, Hatta T, Natsume T, Kawahara H (2018). ZFP36L2 is a cell cycle-regulated CCCH protein necessary for DNA lesion-induced S-phase arrest. Biol Open 7, bio031575.
Payapilly A, High S (2014). BAG6 regulates the quality control of a polytopic ERAD substrate. J Cell Sci 127, 2898–2909.
Ridley AJ, Hall A (1992). The small GTP-binding protein rho regulates the assembly of focal adhesions and actin stress fibers in response to growth factors. Cell 70, 389–399.
Ridley AJ, Paterson HF, Johnston CL, Diekmann D, Hall A (1992). The small GTP-binding protein rac regulates growth factor-induced membrane ruffling. Cell 70, 401–410.
Ridley AJ (2015). Rho GTPase signalling in cell migration. Curr Opin Cell Biol 36, 103–112.
Rodrigo-Brenni MC, Gutierrez E, Hegde RS (2014). Cytosolic quality control of mislocalized proteins requires RNF126 recruitment to Bag6. Mol Cell 55, 1–11.
Sahai E, Garcia-Medina R, Pouyssegur J, Vial E (2007). Smurf1 regulates tumor cell plasticity and motility through degradation of RhoA leading to localized inhibition of contractility. J Cell Biol 176, 35–42.
Sahai E, Marshall CJ (2002). RHO-GTPases and cancers. Nature Rev. Cancer 2, 133–142.
Schaefer A, Reinhard NR, Hordijk PL (2014). Toward understanding RhoGTPase specificity: structure, function and local activation. Small GTPases 5, 6.
Suzuki R, Kawahara H (2016). UBQLN4 recognizes mislocalized transmembrane domain proteins and targets these to proteasomal degradation. EMBO Rep 17, 842–857.
Takahashi T, Minami S, Tajima K, Tsuchiya Y, Sakai N, Suga K, Hisanaga S, Obayashi N, Fukuda M, Kawahara H (2019). Cytoplasmic control of Rab-family small GTPases through BAG6. EMBO Rep 20, e46794.
Tanaka H, Takahashi T, Xie Y, Minami R, Yanagi Y, Hayashishita M, Suzuki R, Yokota N, Shimada M, Mizushima T, *et al*. (2016). A conserved island of BAG6/Scythe is related to ubiquitin domains and participates in short hydrophobicity recognition. FEBS J 283, 662–677.
Torrino S, Visvikis O, Doye A, Boyer L, Stefani C, Munro P, Bertoglio J, Gacon G, Mettouchi A, Lemichez E (2011). The E3 ubiquitin-ligase HACE1 catalyzes the ubiquitylation of active Rac1. Dev Cell 21, 959–965.
Vega FM, Ridley AJ (2008). Rho GTPases in cancer cell biology. FEBS Lett 582, 2093–2101.
Vetter IR, Wittinghofer A (2001). The guanine nucleotide-binding switch in three dimensions. Science 294, 1299–1304.
Vial E, Sahai E, Marshall CJ (2003). ERK-MAPK signaling coordinately regulates activity of Rac1 and RhoA for tumor cell motility. Cancer Cell 4, 67–79.
Wang HR, Zhang Y, Ozdamar B, Ogunjimi AA, Alexandrova E, Thomsen GH, Wrana JL (2003). Regulation of cell polarity and protrusion formation by targeting RhoA for degradation. Science 302, 1775–1779.
Wang Q, Liu Y, Soetandyo N, Baek K, Hegde R, Ye Y (2011). A ubiquitin ligase-associated chaperone holdase maintains polypeptides in soluble states for proteasome degradation. Mol Cell 42, 1–13.
Wei Y, Zhang Y, Derewenda U, Liu X, Minor W, Nakamoto RK, Somlyo AV, Somlyo AP, Derewenda ZS (1997). Crystal structure of RhoA-GDP and its functional implications. Nat Struct Biol 4, 699–703.
Xu Y, Liu Y, Lee JG, Ye Y (2013). A ubiquitin-like domain recruits an oligomeric chaperone to a retrotranslocation complex in endoplasmic reticulum-associated degradation. J Biol Chem 288, 18068–18076.